CHARACTERIZATION OF GEOMECHANICAL POROELASTIC PARAMETERS IN TIGHT ROCKS

A Thesis

by

CLOTILDE RAQUEL CHEN VALDES

Submitted to the Office of Graduate Studies of
Texas A&M University
in partial fulfillment of the requirements for the degree of

MASTER OF SCIENCE

Chair of Committee,	Ahmad Ghassemi
Committee Members,	Eduardo Gildin
	Marcelo Sánchez
Head of Department,	Daniel Hill

August 2013

Major Subject: Petroleum Engineering

ABSTRACT

In petroleum engineering and geophysics, it is often assumed that the rocks are completely rigid bodies with a totally interconnected pore space and that the fluid within the pores does not affect and are independent of the strains in the porous media. These assumptions are often not accurate and also unrealistic because the pore pressure effects are of great importance in all of the geomechanical processes occurring in the subsurface. The hydraulic and mechanical processes are coupled so that the rock deformation causes pore pressure changes and fluid flow (displacement relative to the solid). The time- dependent coupling of the hydraulic and mechanical processes can be described by the theory of poroelasticity. Application of this theory requires the availability of material parameters through experiments. In this work, the main poroelastic parameters are determined for some rock types of interest. The focus of this work is concentrated in low porosity rocks that are commonly encountered.

Experimental procedures under drained, undrained and unjacketed conditions were initially completed in Berea Sandstone. Then, Indiana Limestone, Westerly Granite and Welded Tuff specimens were tested in order to obtain Skempton's pore pressure parameter B, Biot's coefficient of effective stress α, Bulk Modulus and Grain compressibility. Preliminary results suggest that the parameters B, K and α will change in accordance to the permeability and the porosity of the rock, while K_S would depend more on the mineralogy and deposition characteristics of the rock.

DEDICATION

I dedicate this thesis to my mother, who has been with me since the day that I started this journey. Her love and support have kept me faithful through all the adversities that I have faced during my life.

I also dedicate this thesis to all the Claretian Missionaries around the world that are spreading the love of Christ and giving opportunities to those in need.

ACKNOWLEDGEMENTS

I would like to express my sincere gratitude to my advisor, Dr. Ahmad Ghassemi, for his support through the duration of this research project. His guidance, encouragement, dedication and patience were an essential key for the completion of this project. I am very thankful to my thesis committee members, Dr. Marcelo Sanchez and Dr. Eduardo Gildin. The knowledge that I acquired in their classroom was of great importance during the process of this project.

I am very thankful to my laboratory fellows that assisted me during the experimental process, Woodong Jung, Yawei Li, Jihoon Wang and Jihui Ding. I would also like to give thanks to Mr. John Maldonado for his technical support, as well as to his facilities crew, for providing their unconditional assistance. Thanks to Mr. Douglas Tucker for his valuable assistance during the design and manufacturing process included in this project. Last but not least, I would like to thank my friends, especially to Jazmina Urriola for proofreading this document.

TABLE OF CONTENTS

Page

LIST OF FIGURES

Page

LIST OF TABLES

Page

1. INTRODUCTION AND LITERATURE REVIEW

The rocks in the subsurface are deformable porous bodies composed of solid matrix and void spaces. The deformation of the rocks can be elastic, viscous, and/or plastic (Goodman, 1989). The pores in the rocks usually contain fluids with different compressibility to the matrix and the cementing material compressibility. This fluid compressibility has a relevant influence on the overall mechanical behavior of the bulk rock. The matrix is usually composed of solid grain particles and cementing material that connects the rock matrix. In addition to the interconnected pores, there is the existence of dead pores (pores that are not connected to pore space) that do not contribute to the flow, but that do affect the mechanical properties of the rock.

When the pore space in the rock is saturated with fluid and the fluid migrates because of the effect of external stresses and of the presence of gradients in the pore pressure, the state of the stress in the porous media changes, causing a redistribution of the rock stresses, the fluid pressure and also in the volume of the bulk system. In petroleum engineering and geophysics, most of the analysis are made by assuming that the rocks are completely rigid bodies with a totally interconnected pore space and that the fluid within the pores do not affect and are independent of the deformation in the porous media. These assumptions are often not accurate and realistic because the pore pressure effects are of great importance in all of the geomechanical processes occurring in the subsurface. The hydraulic and mechanical processes are coupled so that the rock deformation causes pore pressure changes and fluid flow (displacement relative to the

solid). The time- dependent coupling of the hydraulic and mechanical processes can be described by the Theory of Poroelasticity.

The poroelastic behavior is a result of the solid to fluid coupling and the fluid to solid coupling. The solid to fluid coupling occurs when a variation in the applied stress produces a change in the fluid pressure or the fluid mass. The fluid to solid coupling occurs when a change in the volume of porous material is produced by a change in fluid pressure or fluid mass. These two couplings are assumed to occur instantaneously and that there is no elastic wave propagation, which means that there is no mechanical disturbance that causes oscillations of the particles with respect to their equilibrium conditions. Factors such as the compressibility of the cementation of the matrix, the pores, the solid grains and the pore fluid determine the magnitude of the solid to fluid coupling. The coupling between the solid phase and the fluid phase is described by a set of linear constitutive equations, which are generalizations of the linear elasticity theory and that relates strain and fluid mass changes to stress and fluid pressure changes. In order to use these equations for predicting the mechanical response of rock, the parameters of the porous materials should be determined. In particular, the poroelastic parameters α and B are needed to represent the solid volumetric deformation caused by changes in the pore pressure, and the pore pressure variation in the porous media caused by the application of a mean stress, respectively.

In summary, the theory of poroelasticity resembles the fluid expulsion from a porous media caused by a one-dimensional externally applied load, and can quantify the amount of fluid expelled from a specific volume of porous material. This phenomenon in

a three-dimensional condition would be later better explained in detail in Biot's derivation of the Theory of Poroelasticity (1940) coupled with Darcy's (1856) law for fluid in porous mediua and later developed by Verrujit (1969), Rice and Cleary (1976), and Detournay and Cheng (1993), among others.

2. OBJECTIVE OF THE STUDY

The object of this study is to determine the poroelastic properties of specific igneous and sedimentary rocks that are encountered in geothermal and oil reservoirs. The linear approximations used in the Theory of Poroelasticity will quantify how the state of stresses changes when fluid is extracted or injected in isotropic and fully saturated rock formations. In addition to that, this theory will also help to quantify how the applied loads affect the fluid behavior in the porous media. A set of drained, undrained and unjacketed experiments will be performed to quantify the deformation of the solid phase and the changes in the pore pressure within the elastic regime and during post-peak deformation. With the help of drained and unjacketed tests, we expect to successfully calculate the value of Biot's poroelastic coefficient of effective stress "α".Several approaches will be used in order to prepare the experiments and all of results obtained from each experiment will be compared afterwards. Skempton's pore pressure coefficient B will be calculated from the results of hydrostatic undrained tests that will be performed in different types of rocks and at different pressure conditions. After all the experiments are finalized, all the results will be compared to the results obtained from other authors whenever there is the possibility and in the case that it is not possible, alternative comparisons will be presented by interpreting the mineralogical composition of the rock tested in order to obtain the requested poroelastic parameters.

3. THEORY OF POROELASTICITY

To fully couple the poroelastic theory, the behavior of a material needs to be described by independent parameters, including material parameters and poroelastic parameters, as shown in Table 1. When the rock is considered linear elastic, homogeneous and isotropic, the material constants of the Elastic Moduli and Poisson's ratio needs to be determined because they described the mechanical process that is undergone in the rock. To couple the mechanical and hydraulic processes, variables such as the Biot's effective stress coefficient and Skempton's pore pressure parameters are required, as well as parameters such as drained and undrained bulk modulus, and shear modulus. The focus of this work is to determine the poroelastic parameters $\propto$ and B experimentally, under hydrostatic loading. This special case of hydrostatic loading for the poroelastic theory was fully explained by Geerstma (1957) and Zimmerman (1991).

Table 1: Poroelastic Parameters obtained using different tests.

Options of Required Parameters	**Number of parameters that need to be obtained from the drained laboratory test**			**Number of parameters that need to be obtained from the undrained laboratory test**				$\propto$	**B**
	E	**υ**	**K**	**G**	**E_u**	**$υ_u$**	**K_u**		
Option 1	1			0				Use both	
Option 2	2			1				Select either $\propto$ or B	
Option 3	1			2				Select either $\propto$ or B	
Option 4	0			2				Use both	

The poroelastic coupling can be described by a set of linear constitutive equations that relates strain and changes of fluid mass to stress and fluid pressure changes. In order to make the constitutive equations applicable, the rock is considered a linear isotropic and poroelastic material. The solid to fluid coupling depends primarily in the compressibilities of the material framework, the solid grains, the pore fluid and the porosity.

It is imperative to recognize the role of the pore fluid in the rock mass. The changes of fluid mass or pressure in the porous material produce strains in the volume of the bulk. The poroelastic theory implies that the changes in the pore fluid are exclusively caused by external stresses and that the free strains are not a cause of poroelastic stresses.

Two different approaches can be used to describe the poroelastic behavior of the porous media: first, the rock is considered a "continuum", where the fluid and the bulk are considered as fully integrated, and a micromechanical approach where the fluid and the solid contributions are individually accounted.

As a continuum, the constitutive equations for the porous media in the Biot's formulation assumes elasticity, which means that there is linearity between the stress and the strain, and also that there is no dissipation of energy during the loading and unloading process, leading to the total reversibility of the deformation process. Generally, the isotropic material response can be written by reorganizing the stress-strain relations for porous materials as:

$$\varepsilon_{ij} = \frac{\sigma_{ij}}{2G} - \left(\frac{1}{6G} - \frac{1}{9K}\right)\delta_{ij}\sigma_{kk} + \frac{K}{3\alpha}\delta_{ij}p_p$$

In order to assume reversibility of the deformations, the work increment needs to be an exact differential:

$$dW = \sigma_{ij}d\varepsilon_{ij} + p_p d\zeta = \varepsilon_{ij}d\sigma_{ij} + \zeta dp_p$$

For an isotropic poroelastic material, the hydrostatic poroelastic volumetric behavior can be summarized to:

$$\varepsilon = -\left(\frac{P_c - \alpha p_p}{K}\right)$$

$$\zeta = -\left(\frac{P_c K}{\alpha} - \frac{\alpha p_p}{BK}\right)$$

In the micromechanical approach the contributions of the solid and the fluid are separated. It is useful in order to obtain an additional insight on the interaction of solid-pore-fluid system, even beyond the non-linear range of elasticity. According to this approach, the volumetric response of porous material to any applied stress can be described by the linearity between stress and strains, we can write that:

$$\frac{\Delta V}{V} = -\left(\frac{P_c - \alpha p_p}{K}\right)$$

And if separated into two loading components (for the fluid and for the solid), it can be written that:

$$\frac{\Delta V}{V} = -\left(\frac{P_c}{K}\right) - \left(\frac{p_p}{K_s}\right)$$

To finalize decompose the contributions of the fluid and the solid in the deformation of the porous material.

3.1 Biot's Coefficient of Poroelasticity α

The poroelastic response of geomaterials was first described by Karl Von Terzaghi in 1943 in his one- dimensional consolidation theory for soils and rocks. In this theory, the geomaterials are presented as incompressible linear elastic, homogeneous and isotropic materials that dissipate the pore pressure in the vertical direction due to an applied vertical stress over a unit of soil (Terzaghi, 1943) . In the experiments utilized to develop this theory, Terzaghi fully saturated a soil specimen, confined it laterally in a cylinder and then an axial constant load was applied. Excess pore pressure developed within the sample during the fluid migration and then the consolidation equation was derived as the diffusion equation for excess for water pressure, as shown below:

$$\frac{\partial p}{\partial t} = c\frac{\partial^2 p}{\partial z^2}$$

Where *c* is the consolidation coefficient, *t* is time and *z* is the vertical distance in the soil column.

In Biot's Theory, the knowledge of the effective stresses is imperative. The effective stress for failure analysis is calculated using Terzaghi's effective stress definition:

$$\sigma' = \sigma - p$$

Where σ' represents the effective stress, σ the total stress and p the pore pressure. However, experimental and theoretical analysis shows that during rock deformation, it is necessary to take into consideration Biot's coefficient of effective stress:

$$\sigma' = \sigma - \alpha p$$

Where α is Biot's effective stress poroelastic parameter, which varies from 0 to 1, depending on the rock characteristics. The coefficient α can be defined as a correction factor, that depends on the rock texture (grain arrangement and the cementation between the grains) that prevents pore fluid from fully carrying an applied load, so that Biot's constant α determines the amount of stress carried by the rock matrix when a pore fluid is present. When α=0, the total stress applied to the porous system is fully carried by the rock solid grains and cement and when α=1, the stress is carried by both the fluid and the solid. The higher the coefficient of effective stress is, the more incompressible is the grain and the conditions are likely to be isotropic. This case is particularly true for Terzaghi's observation for soil materials.

From the micromechanical approach of the theory of poroelasticity, we know that the coefficient of effective stress α can be expressed in terms of the ratio of compressibility of the rock as a bulk to the compressibility of the grains (so that it accounts for the porosity that is not interconnected porosity).

$$\alpha = 1 - \frac{K}{K_s}$$

The above expression can be used to calculate α by first measuring K_s and K independently.

From the continnum constitutive equations and the micromechanical approach, we can define the parameter α as the ratio of the change of volume of fluid to the change of the volume of the rock under a stress change. A common experimental procedure use to obtain α coefficient is to carry out a drained test under increasing hydrostatic stress (at a constant rate). During the test, the fluid tends to migrate from the saturated rock specimen as a response to the incremental pressure in order to maintain a constant pore pressure, and the volume of fluid expelled from the specimen is recorded along the duration of the test. The parameter α traditionally is calculated as the ratio of the variation of the pore volume with respect to the total volume change and that can be better expressed as:

$$\alpha = \frac{\Delta V_p}{\Delta V_b}$$

In the original Biot's theory, the poroelastic coefficients were presented in a different way as these days, using quite different parameters. The coefficient of effective stress $\propto$ was originally defined as the product of the Bulk Modulus with the poroelastic expansion coefficient 1/H, and that describes how much a change of pore pressure also changes the bulk volume, while the applied stress is kept constant under controlled undrained conditions. In the experimental method we will describe the tests to be performed in order to calculate this poroelastic parameter. It is possible to determine the poroelastic coefficient of effective stress α by using Biot's original coefficients of poroelasticity as early described by Biot and as it is shown below:

$$\alpha = \frac{K}{H}$$

Where K is the bulk modulus of the rock and $1/H$ is the poroelastic expansion coefficient, which relates the volumetric strain to pore pressure changes under a constant state of stress. To make this calculation effective, we need to obtain both poroelastic parameters from different experimental procedures. During the first procedure, we could determine the bulk modulus by loading and unloading hydrostatically the rock specimen at a constant pore pressure in drained conditions. The bulk modulus could then be calculated as:

$$K = -V\frac{\delta Pc}{\delta V}$$

where V is the bulk or total volume of the rock specimen, and Pc is the confining pressure at which the specimen is subjected. Bulk modulus K can be used to determine α because it is a parameter purely independent from the pore pressure and it fully responds to the elastic behavior of the material. Under pure elastic conditions, the Bulk modulus of any porous material is a mechanical property and if the pore fluid conditions are not changed ($\delta Pp = 0$), the volumetric change observed can be attributed exclusively to the external applied stresses, rather than to the pore pressure conditions present. The change in the bulk volume in response to a change in the state of stress will be the same in a saturated or dry specimen, as long as drained conditions are prevalent. In order to obtain the parameter 1/H the confining pressure is held constant at a specific stress level, and the pore pressure is changed at a constant rate. It is important to always keep a safe positive effective stress to prevent migration of the pore fluid into the triaxial cell, which

will be achieve by setting the specimen into a considerably high hydrostatic state of stress and always keeping the maximum pore pressure applied under this selected hydrostatic stress. The volumetric strain in the specimen is recorded simultaneously as the rock deforms in response to the change in the pore fluid conditions. The poroelastic expansion coefficient *1/H* could be calculated as:

$$\left.\frac{\delta\varepsilon}{\delta p}\right|_{\delta Pc=0} = \frac{1}{H}$$

After the bulk modulus K and the expansion coefficient 1/H are obtained from their correspondent tests, the results from the drained test and the coefficient of expansion test will be combined and Biot's effective stress coefficient α correspondent to various stress level can be calculated in an independent manner.

3.2 Skempton's Pore Pressure Parameters

Skempton's coefficient is a pore pressure buildup coefficient used to measure the effects of pore pressure increase during a sudden application of a compressive stress (Skempton, 1954). Making the assumptions of isotropic stress conditions and a linear elastic material, under undrained conditions there is no fluid migration from the controlled volume of porous media and the effect of external stress over this volume will change the pore pressure through volumetric change of the rock and the fluid, as the increment of stresses happens rapidly and the volumetric change does not occur at a pace that allows the fluid to redistribute in the porous media. With compressional external forces, the constraint in the volumetric deformation will impact in fluid response and the

pore pressure will build up as a response of the increment in applied stress. Skempton's pore pressure coefficients *A* and *B* will determine the fraction of the change in pore pressure as a function of the change in the external stress and vice versa, and can be expressed as:

$$\Delta p = B(\Delta\sigma_3 + A\Delta\sigma_d)$$

where $\Delta\sigma_d = (\Delta\sigma_1 - \Delta\sigma_3)$ is the change in the deviatoric stress, $\Delta\sigma_1$ and $\Delta\sigma_3$ are the changes in axial and confining stresses respectively. The Skempton's *A* parameter represents the parameter at failure (contribution of the deviatoric stress), while the parameter *B* is a function of the saturation in the porous media. The value of *A* might be negative in the case of a tensional test and positive in a compressional test, and *B* value varies within a range from 0 to 1. In summary, Skempton's pore pressure coefficient measures how the applied stress is distributed between the skeletal framework and the fluid. For the purposes of our study, we will only base our analysis in hydrostatic conditions, therefore only the analysis of the parameter *B* will be included in this study.

4. PETROPHYSICAL PROPERTIES AND MINERALOGY

Rock specimens of Berea Sandstone, Indiana Limestone, Westerly Granite and Welded Tuff were used for the tests covered in this study. Berea Sandstone is a sedimentary rock composed basically of sand-sized (1/16 mm to 2 mm) regular-shaped particles that are cemented primarily by silica. Based on previous triaxial tests, the 1.00" D x 2.00" L specimen has a unconfined compressive strength of 43≈55 MPa, a porosity of 18%≈20%, a brine permeability of 60 mD to 100 mD and a dry bulk density of 2.2 g/cc, both measured by the core plugs supplier, Kocurek Industries in Caldwell, Texas.

The Indiana Limestone is a very pure, massive calcium carbonate, even textured and medium grain rock that contains calcite-cemented fossils. This rock has a granular texture and the grains range from fine (<1 mm) to coarse (>3 mm) and it is well sorted and even grained. The average fossil size is 0.2 to 0.5 mm and it is cemented with calcite. The bulk volume of the Indiana limestone is mostly compose of echinoderm pieces and bryozoan fragments in almost half of its volume, calcite matrix and other miscellaneous fossils, where the matrix calcite is clear and unpitted. In a minor quantity, it can also be encountered grains of quartz, feldspar, and hematite or magnetite. The bulk is composed of approximately 18-19 percent of void space, with only 0.8 to 1.4 percent can be accounted as dead pores. The specific gravity is 2.37 and the unconfined compressive strength is approximately 34.6 MPa and a measured brine permeability of approximately of 3 mD, measured by Kocurek Industries, Inc.

The third type of rock used was Westerly Granite which was obtained from Westerly, Rhode Island. Westerly granite is a light-gray with tints of blue to pink granitic rock, pink-weathering, equigranular, fine-grained, massive, aplitic granite, composed of oligoclase or albite (31.4%), quartz (27.5%), and K-feldspar (39.5%), with minor biotite (4.9%) and accessory muscovite, magnetite, allanite, and sphene. The rock low porosity (0.9%) and the homogeneity of the minerals make it a very popular specimen in experimental rock mechanics and a very suitable type of rock for our purposes. The lack of interconnectivity between the cracks makes it a very low permeability rock. Because of its origin, this type of rock has also microcracks within the minerals ranging from apertures of 0.7 to 0.002 micrometers in width, with a mean crack aperture of 0.015 micrometers. The measured unconfined compressive strength for this rock ranges from 200 MPa to 245 MPa.

The last type of rock used is Welded Tuff, where three different specimens were tested for the purpose of this work. The specimens were recovered from a location near the Newberry Volcano, Oregon from coreholes GEO N-1 and GEO N-2 (Figure 3) and obtained from the University of Utah Core Laboratory. The first specimen labeled N1 4348 1V and its thin section is displayed in Figure 1. This rock is an intermediate tuff or rhyolite tuff, with massive microcrystalline to cryptocrystalline minerals. They have an argillitic texture with intermediate composition between porphyritic rhyolite and aphanitic andesite. The argillitic material texture usually forms firm to slightly soft and ductile rock. Bright colored fragments that are plagioclase minerals within a buff color clay matrix were observed, with a very fine grained groundmass. This rock has high clay

content, making it fine-grained and it also has large crystals, accompanied by small-sized vesicles like meringue. The recovered core has a low porosity and low permeability. This specimen has a permeability of approximately 1.17E-02 md to 5.21E-02 md and a porosity ranging from 12.38% to 16.71%.

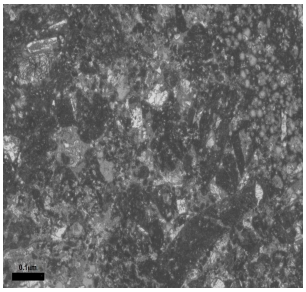

Figure 1: Thin section N1-4348.

The second Welded Tuff specimen tested is labeled N1-4013-3H and its petrographic thin section can be observed in Figure 2. This rock has a texture that is porphyritic to aphanitic and with an intermediate composition between porphyritic rhyolite and aphanitic andesite. This rock is a dacite, or lithic tuff with pre-dominantly andesitic composition with glassy light gray matrix. It also contains micro-porphyritic feldspar, quartz, and small amount of amygdales, green smectite/clay and zeolite. The permeability for this rock ranges from 1.68E-04 to 6.0E-04 md and the porosity is approximately 1.79 to 3.35%.

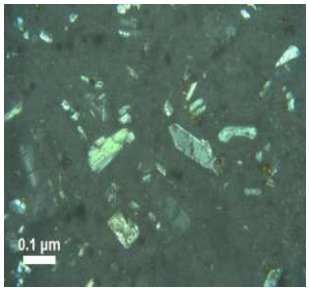

Figure 2: Thin section N1-4013.

The last rock specimen used is labeled N2-4281-4V. This rock has an aphanitic texture and is intermediate in composition between porphyritic rhyolite and aphanitic andesite. It is an intermediate tuff or rhyolite tuff, containing massive microcrystalline to cryptocrystalline minerals. The rock also contains bright colored fragments that are plagioclase minerals within a buff color clay matrix and has high clay content. Small sized vesicles are observed and fractures are cemented with calcite. The measured permeability for this rock was approximately 7.40e-5 md and the porosity between 4.99% and 6.44% measured using the gas porosimeter.

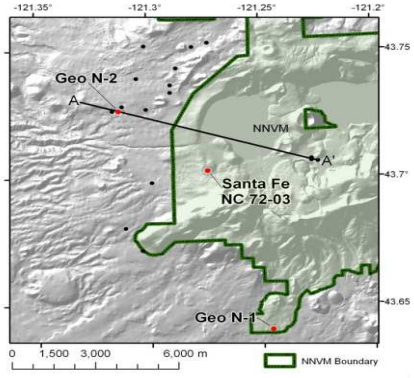

Figure 3: Location of coreholes Geo N-1 and Geo N-2.

5. EXPERIMENTAL PROCEDURE

Poroelastic laboratory experiments were carried out using the Terratek Triaxial System (Figure 4) and the GCTS Triaxial System RTX-1500 (Figure 5), both with an axial load capacity of 1,500kN, a confining and pore pressure limit of 140 MPa and located at the Rock Mechanics Laboratory in the Petroleum Engineering Department at Texas A&M University. In the GCTS triaxial system, the confining pressure is provided by hydraulic oil DTE-25, while for the the Terratek triaxial system the confining pressure used is the mineral oil Paratherm NF®. With both equipments the pore fluid used were deionized water and Paratherm NF ®, depending on the test to be performed. For the undrained and the drained tests the system used was the GCTS Triaxial System RTX-1500, while for the unjacketed test the system used was the Terratek Triaxial System.

Figure 4: Terratek Triaxial System.

Figure 5: GCTS triaxial system RTX-1500.

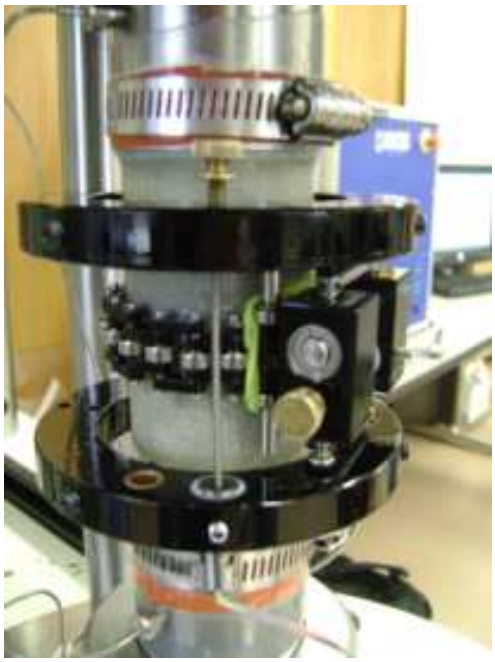

Figure 6: Specimen installation.

Figure 7: Syringe pump used to reduce the external fluid volume.

Before carrying out any experimental procedure, all the specimens were photographed, and then they were dried in the oven at 100°C for about 14 hours in order to reduce the environmental moisture. After each specimens were removed from the oven they were saturated using the imbitition method. This method consists in displacing the air trapped within the pores of the rock specimen by changing the capillary pressure between the grains and allowing a wetting fluid (deionized water or mineral oil) to go into the pores.

5.1 Equipment Design

It is important to take into consideration the effect of the dead volume of the drainage system in the triaxial cell while evaluating poroelastic properties of saturated porous media. The compressibility of the drainage system has an influence with the measured pore pressure and volumetric strain during mechanical loading in a conventional triaxial cell. Ghabezloo and Sulem (2009) proposed a correction to adjust the effects of dead volumes in the drainage system during undrained isotropic compression tests or during undrained heating tests. They used a parametric study in order to demonstrate that the porosity and the drained compressibility of the tested material and the ratio of the volume of drainage system to the fluid volume of the rock core specimen are the parameters that influence the error induced on the measurements obtained from these tests. In this study, they are limitations with respect to the porosity of the rock specimens, where the results showed that for rocks with porosities under 10% the error in the Skempton's pore pressure parameter might be over 40%. We conclude

that this method is not applicable for our case, where our specimens have porosities between 0.5% and 4.0%, therefore the design of a system with volume constraints was imperative in order to continue with the experimental phase.

A pore pressure measurement system was designed to complement with the triaxial cell in order to measure with a high degree of accuracy the poroelastic parameters in low porosity specimens. The purpose is to design a system that can have an unutilized fluid volume of less than 4% of the void volume in the specimen, and at the same time that might allow having a proper monitoring of the pore pressure in the rock specimen. The existing platens are not suitable for our measurements because they lack of a monitoring system, such as an embedded pressure sensor.

The most practical way of reducing the unused volume is by measuring the pore pressure reading as close to the rock specimen as possible. A viable way to reduce this volume is to place the pore pressure transducer within the steel platen that holds the rock specimen. The possibility of drilling the existing platen was considered, but not used because it should preserved in original conditions for other tests and because it was thermally treated, and might be not very favorable for molding and welding. For this purpose, a bottom platen was manufactured using steel 4140 as a base material. The material was provided in a prehardened condition and heat treated to a medium hardness by annealing at a temperature of 830^{o}C. The modulus of elasticity for this material is approximately 200 GPa, the density is 7810 Kg/m^3 and the yield and tensile strength are 570 MPa and 850 MPa respectively. This is a very machinable material that can deliver toughness, good torsional and good fatigue strength. This material is very popular given

that it is commonly used for multiple industrial purposes; therefore it was available immediately. This new platen was designed following the dimensions of the original platen (see Figure **8**), with the difference that the new platen will composed of a hollow cylinder if compared to the original, which is completely solid at every cross sectional location.

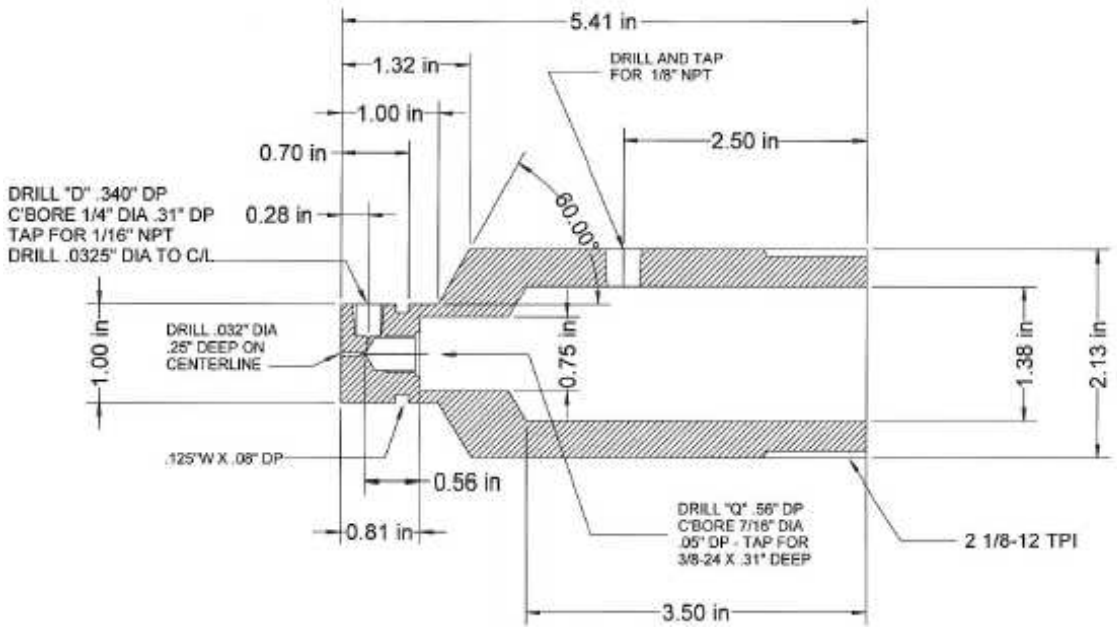

Figure 8: Poroelastic platen blueprints.

A pressure miniature transducer Model S manufactured by Honeywell Inc, was installed in the inner part of the platen from the bottom part and the platen was drilled laterally to bypass the electric cables. This transducer has a pressure capacity of 10,000 psi and a temperature operating range from -54^{o}C to 149^{o}C.

The hydraulic setting of the system was set to accomplish a minimal unutilized fluid volume when possible. The orifice design that will conduct the fluid through the pores was verified for the parameters of fluid turbulence and friction head loss. Learning from past experiences and using information from several publications, the external fluid volume will be kept as its minimum, at a value of 4% of the total pore volume in the specimen. For the case of a 1" x 2" specimen with a porosity of 2%, the total volume of external fluid allowed will be of 0.0025 in^3. This unutilized fluid volume needs to be redistributed along the tubing and the accessories. The tubing used will have an OD of 1/16" and with an ID of 1/32". This ID will allow an external volume to be distributed along a distance of 3.28 in, including the piping within the platens and the external tubing. A smaller internal diameter was not explored because there is no availability in the manufacturers and to avoid as much friction head loss as possible. Continuous to the tubing, a 1/8" lift check valve was installed in order to build the control volume. A needle valve will be installed next to each check valve to aid to depressurize the system after the test is performed. The orifice within the platen will allow a pore volume of 5.36 x 10^{-4} in^3, which is about 1.71% of the total fluid volume in a 1" x 2" specimen that has a porosity of 2%.

The considerations taken for the design of this system includes a broad range of parameters, from mechanical to the hydraulic properties in the different elements that conforms the system. For the structural design of the platens, the load resistance factor design method (LRFD) was used. The structural members were design for compressive strength, compressional buckling and minimum elastic deformations. For the

compressional design, a cross-sectional area of steel of 0.689 in^2 is required, where the minimum available is 0.785 in^2, for an ultimate load of 50.28 kips. The Internal diameter of the base of the platen was set to a maximum dimension of 1.90 in (a wall thickness of 0.22 in is required. The factor of safety against buckling was computed at 1.13 for the OD of 1.00 in and 171.00 in for the section of the platen with an OD of 2.12 in. Figure **9** shows a diagram of the pore pressure measurement system.

The backside of the transducer will be sealed by using a 1/8" male NPT to 1/8" tubing connector in the corresponding orifice (Figure 10) and passing the electrical shielded cables through a thermocouple connector up to the connectors located in the inner part of the cell, specifically to outlet #4 (see Figure 11) in the GCTS pressure vessel, and sealing the open extremes with the anaerobic thread sealant SWAK, with a viscosity of 100 000 cP, a temperature rating of -65°F to 350 ° F and a working pressure of 10,000 psi.

The electrical excitation for the subminiature transducer will be provided by the SCON-2000, the same controller for the triaxial testing machine, as well as the output signal for the outcoming pore pressure measurements.

To summarize, the system will be composed by a Teledyne Isco 100 DM syringe pump that will provide the initial pore pressure to the specimen in the inlet, the bottom platen discussed above and the GCTS RTX-1500 triaxial testing system that will provide axial and confining loads. There will not be a pore pressure outlet for the undrained case; therefore all the pore pressure will need to be released using the inlet. This will be done by bleeding the check valve that controls the volume, using a pressure of 41.38 MPa.

The existing top platen will be used, and its orifice will be closed using a 4140 alloy cap, to prevent increasing the dead volume of pore fluid.

After the equipment assembly, a calibration work will be performed to the subminiature transducer. The new poroelastic platen installed in the GCTS Triaxial Testing System without any specimen or top platen to allow the confining oil to pressurize the subminiature transducer, and then the cell filled up with confining oil. Before beginning the calibration, a leaking test would be performed to predict any apparent leaking of the cell pressure fluid into the platen because such a leak may cause damage to the backside of the pressure transducer that because of size limitations in the design could not sealed to resist high pressures. After the platen is installed and the vessel closed, the cell pressure would be increased to 7 MPa after the axial actuator is set to the lowest position possible to avoid any air entrapment that might prevent the cell from being filled and to ensure that the cell pressure could be increased. After the cell pressure is raised, it would be again decreased to 0.5 MPa, and then the confining oil was removed from the cell. After the confining oil was cleared out from the triaxial cell, the platen is unscrewed from the base of the cell to detect the presence of confining oil into the bottom of the hollow cylinder, an indicative of oil leaking into the platen. This deficiency was corrected by drilling a groove in the base of the platen, as shown in Figure 12. The groove was manually milled to fit a 130 BUNA O-ring, which will seal the contact of the bottom of the platen with the base of the triaxial vessel. A spanner hole was also added in the lateral faced of the platen to provide torque by using an adjustable 1/4”-3” pin spanner.

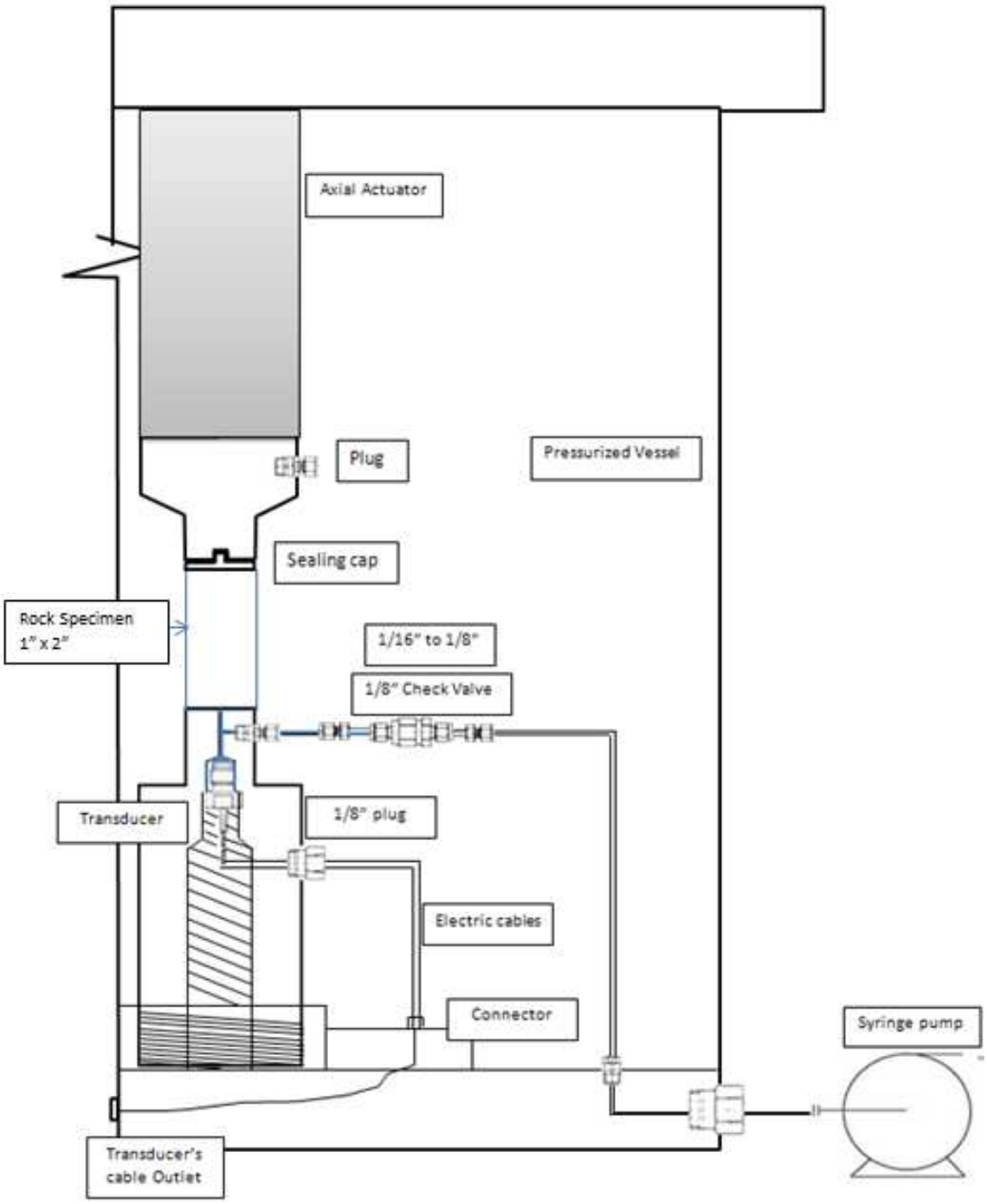

Figure 9: Pore pressure measurement system.

Figure 10: Manufactured steel platen.

Figure 11: Electrical ports where the pore pressure transducer is connected.

Figure 12: Seal made with an O-ring to prevent leakings.

6. TEST RESULTS

After the new experimental setup was completed, a set of experiments were performed with this new setting described above. Drained, undrained and unjacketed hydrostatic poroelastic tests were conducted in Indiana Limestone, Berea Sandstone, Westerly Granite and Welded Tuff. These new set of experiments were accompanied with an update in the procedures that was forced by the constraints introduced with the new design. One of the main improvements made was during the saturation process. The saturation process was made by cyclically loading the specimen after the sample was completely saturated, as described in the previous section. The degree of saturation in the specimen was determined by injecting pore fluid at a constant pressure through the bottom platen, always making it smaller than the confining pressure. The pore pressure within the specimen was monitored by plotting the real-time pore pressure measurement as a function of time. When the pore pressure was observed to be constant, the external valve between the triaxial cell and the syringe pump that provides the pore fluid was closed. After the valve was closed, the pore pressure was monitored for an initial period of 10 minutes. If supposedly the specimen was not fully saturated, the pore pressure within the platen (located at the inlet part of the specimen) will start dropping. This occurred because the injected fluid was flowing into the specimen, due to the lack of saturation in the porous media. In this case, the valve was open and more fluid was allowed into the system and the closed again. If after a lapse of 10 minutes the pressure at the inlet is not presenting a noticeable drop, it means that no more fluid is allowed into

the specimen and that the pressure is evenly distributed along it. A pressure drop was considered as negligible if after the ten minutes period it has a difference of 2% or less, if compared to the initial injected pressure.

6.1 Skempton's Pore Pressure Parameter B

6.1.1 Undrained Test

For an undrained hydrostatic test, the rock specimen was assembled as observed in Figure 13, where the pore fluid was provided by the ISCO 100 DM. The specimen was saturated by injecting pore fluid from the syringe pump into the bottom platen and the pore pressure was monitored using the miniature transducer installed in the bottom platen. When the pore pressure in the bottom platen reaches the target pressure applied using the syringe pump, the ball valve showed in Detail 1 of Figure 13 between the specimen and the syringe pump was closed in order to create undrained conditions in the specimen, by not allowing any pore fluid to enter or leave the sample. It was determine that the sample was fully saturated when the miniature pore pressure transducer reads a difference of less than 2% with the pore pressure prior to shut off the valve.

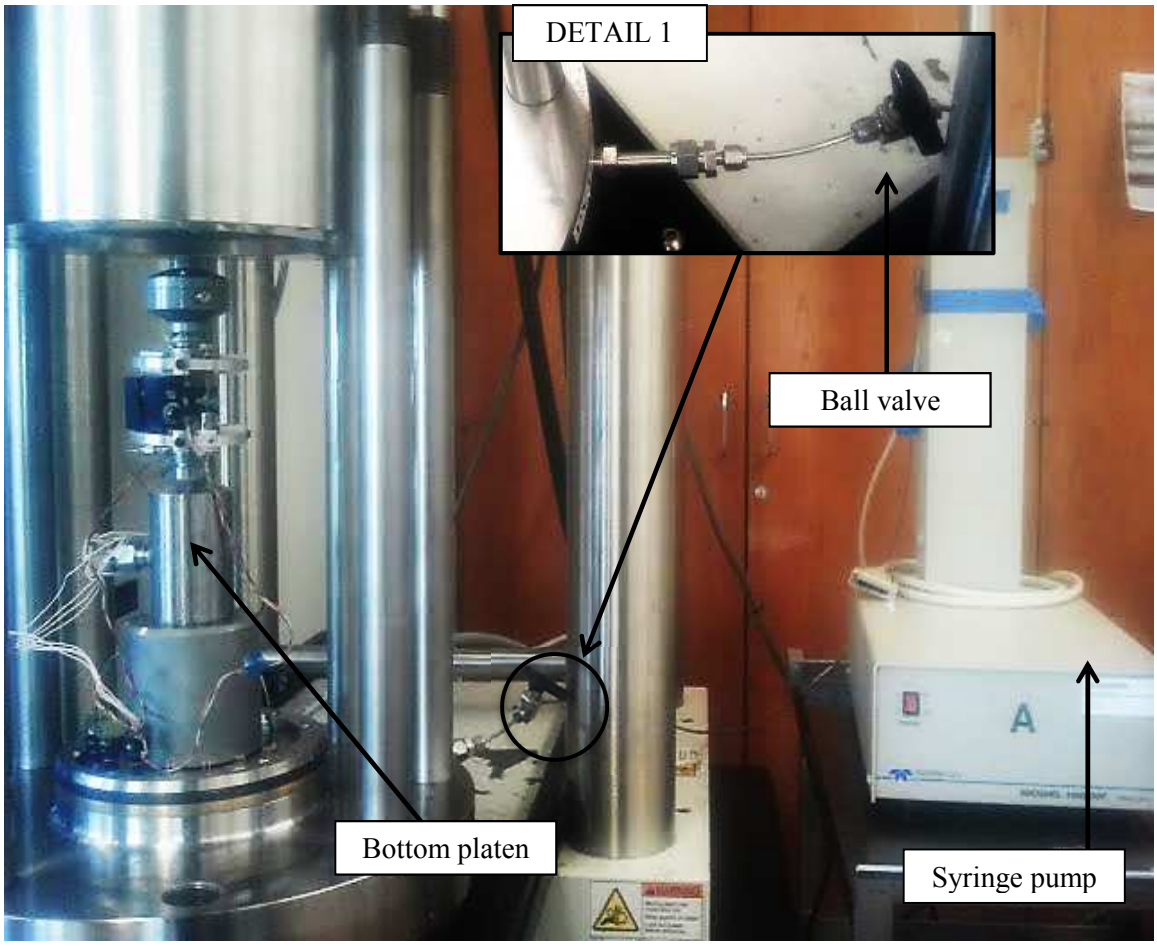

Figure 13: Undrained test set-up.

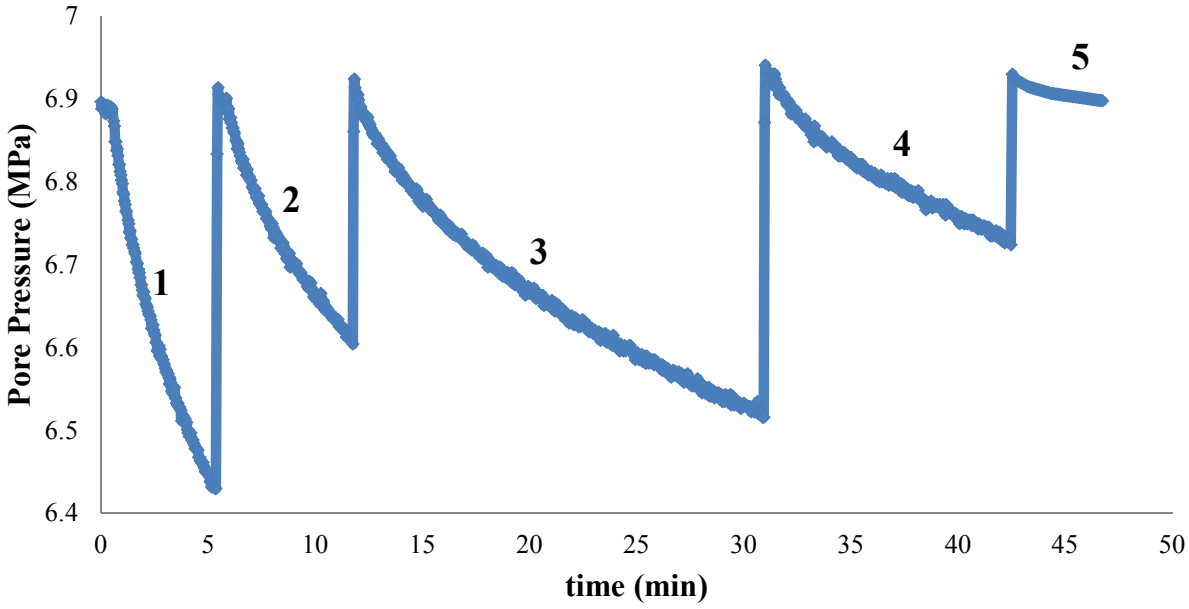

Figure 14: Saturation process before the test.

Figure 14 shows the saturation process prior to the test. The ball valve was closed when t=0 and the pore pressure reading was 6.90 MPa. After the valve was closed, the pressure started dropping as can be seen in stage 1. At the end of stage 1 the valve was reopened and more fluid was allowed into the system and the valve was close before stage 2. The procedure was followed in order to give enough time to the fluid to diffuse through the porous media and to displace from the pore fluid outlet into the sample. This procedure was repeated for stages 3, 4, and 5. In stage 5 the pressure drop in 5 minutes was less than 2% and the valve was closed to finally finish the saturation process. After this point, the pore pressure stop dropping and it can be noticed that in stage 5 the pressure decline approached a horizontal slope. It is also noticeable that the pressure drop in time was more severe in the first stage, and started getting mild every time that

the valve was open and more fluid allowed into the specimen. Finally, in stage 5 the sample can be say to be saturated because of the minimal pressure drop and rapid stabilization of the pressure during theprocess.

After the saturation process was finished and the ball valve definitely close, the cell pressure was increased at a rate of 0.33 MPa/min and all data was recorded every 1/10 seconds. The recording time for the pore pressure change was set at 30 seconds because it was observed that if the increments of time were set very small, then the change in the pore pressure might result in very small numbers or even negative increments, that resulted in misleading plots with B values that were negative or close to zero. As a result, the maximum peak values of B cannot be noticed unless a further filtering of the data is done, which can be very time consuming. The test was set to start at a hydrostatic confining pressure of 10 MPa and a pore pressure of 6.9 MPa (1000 psi), until the peak value of B was achieved. Figure 15 and Figure 17 show the pore pressure response in hydrostatic condition for Berea Sandstone and Indiana Limestone, respectively. Figure 16 and Figure 18 show the value of the undrained parameter B changing with hydrostatic pressure for Berea Sandstone and Indiana Limestone respectively. In both cases, the pore pressure parameter B peaked within the ranges of the experiment, with maximum values of 0.64 for Berea Sandstone and 0.54 for Indiana Limestone. It can be observed that the pore pressure response increased substantially if compared to the results previously obtained, and also they are similar values to results previously obtained by other authors, which are compared in Table 2. From this comparison, we can infer that our measurement of the coefficient B was accurate for

both cases, and that we could proceed with the experiments in the low porosity rocks object of our study.

Table 2: Comparison of B values with other authors.

Rock Specimen	Skempton Pore Pressure Parameter B		
	This Work	Hart	Akbarnejad-Nesheli
Berea Sandstone	0.64	0.84	0.55
Indiana Limestone	0.54	0.4	0.46

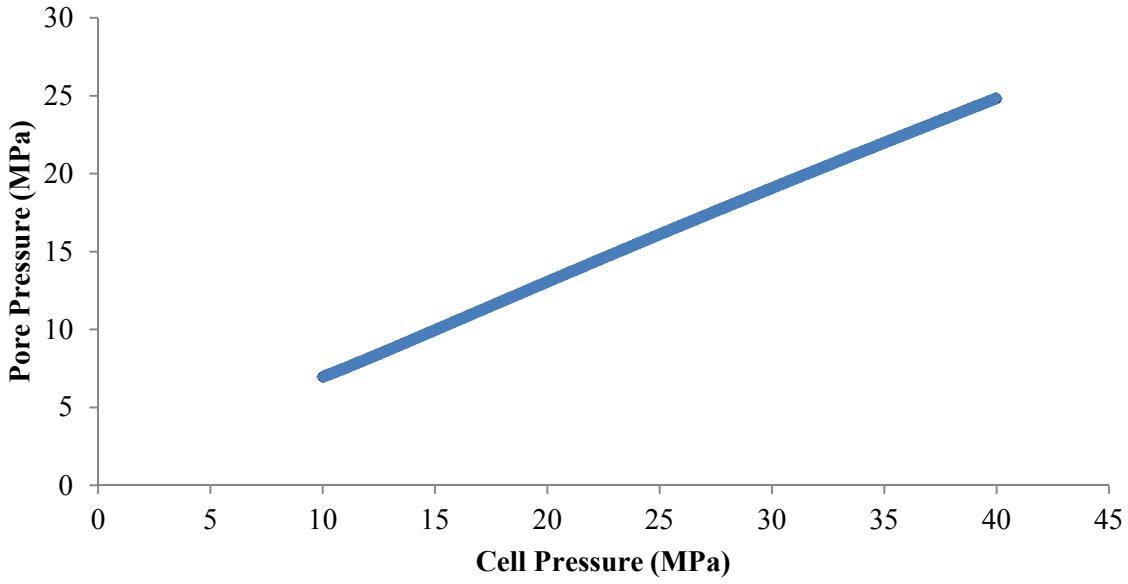

Figure 15: Pore pressure response in undrained test in Berea Sandstone.

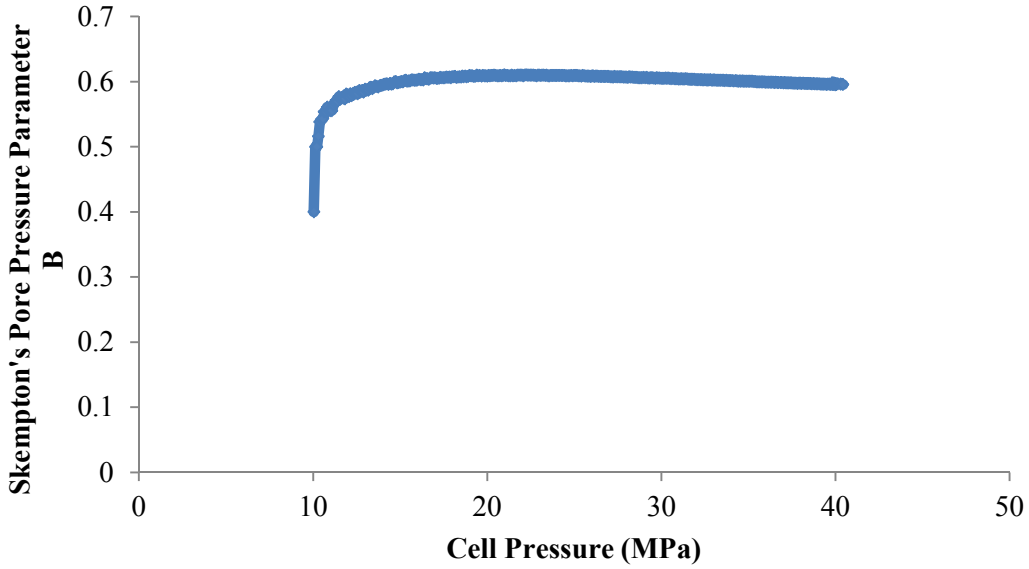

Figure 16: Skempton's pore pressure Parameter B for Berea Sandstone.

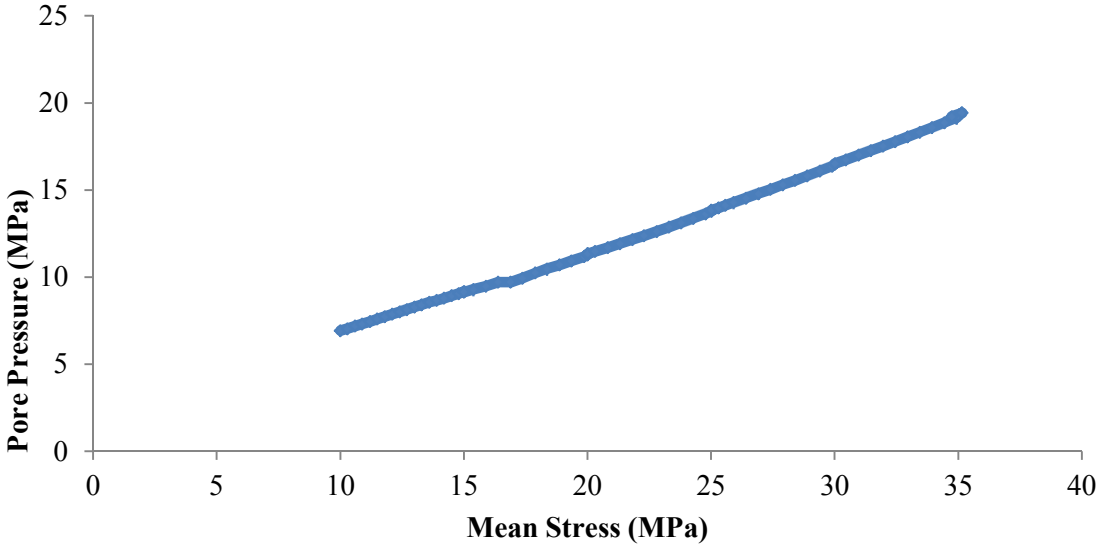

Figure 17: Pore pressure response in hydrostatic undrained test in Indiana Limestone.

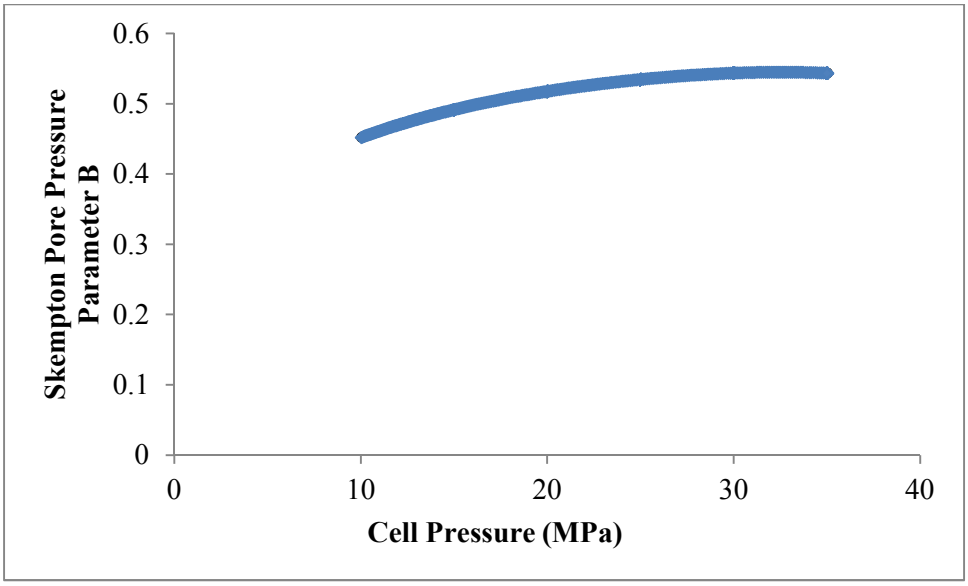

Figure 18: Skempton's Pore Pressure Parameter B for Indiana Limestone.

While an undrained experiment was performed for Westerly Granite, it was not possible to obtain results from this test. When the rock specimen was loaded at the beginning of the test, the induced pore pressure responded by increasing abruptly and overcoming the cell pressure. As a result, the effective stress became negative and the heat shrink could not resist the difference in pressure when the rock sample fragmented, as observed in Figure 19. This phenomenon was first observed in saturated soils and is known as the Mandel-Cryer effect and it was first observed by Mandel (1953) in triaxial soil specimens and by Cryer (1963) for spherical specimens. It is caused by an irreversible decrease in the elastic stiffness in the skeleton of the material and by incompatibilities of the pore fluid and the deformations of the porous solid skeleton that leads to the increment of the pore pressure field in the pores (Selvadurai, 2004). The

stresses are transferred to the interior of the cylinder and the undrained buildup in pore pressure decay takes longer than in the coupled pore pressure diffusion.

Figure 19: Mandel- Cryer effect in Westerly Granite.

By comparing the values obtained in our experiments to values obtained by other authors, we can determine that our equipment is accurate enough to determine the pore pressure response for rock specimens with lower porosity. The same procedure used for the Berea sandstone and Indiana limestone was followed in order to monitor the pore pressure response for Welded tuff specimens labeled N1-4348-1V, N2-4281-4V and N1-4013-3H.

In Figure 20 is shown the hydrostatic undrained test performed in order to calculate Skempton's pore pressure parameter B for the Welded tuff specimen N1-4348-1V. The initial stage of this test from 10 MPa to 13 MPa of confining stress did not presented drastic changes in the pore pressure response, staying at almost the same initial pore pressure of 8.33 MPa. The highest pore pressure increment during the test

was observed at the interval that comprises from 13 MPa to 30 MPa of confining pressure, where the peak value of increment in the pore pressure is observed. From 30 MPa to the end of the test at 40 MPa the slope becomes less steep and almost constant.

The pore pressure response for the specimen N2-4281-4V is displayed in Figure 21. The pore pressure increment responded linearly from the beginning of the test until the confining pressure of 18 MPa, when the pore pressure increased exponentially to reach it maximum value at 21.6 MPa. In the last interval, from the peak slope value until the end of the test, the pore pressure changed almost linearly and at a slower rate.

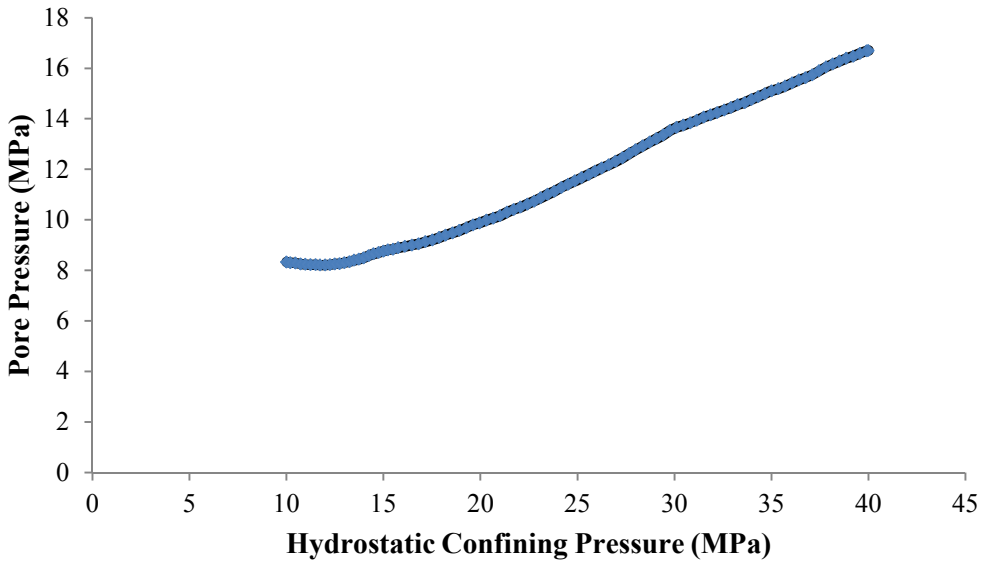

Figure 20: Hydrostatic Undrained test for specimen N1-4348-1V.

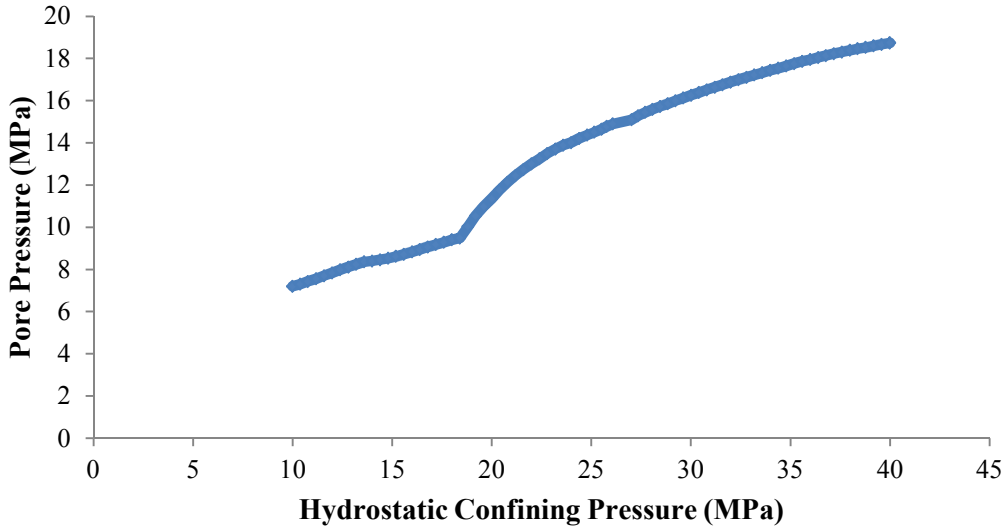

Figure 21: Hydrostatic Undrained test for specimen N2-4281-4V.

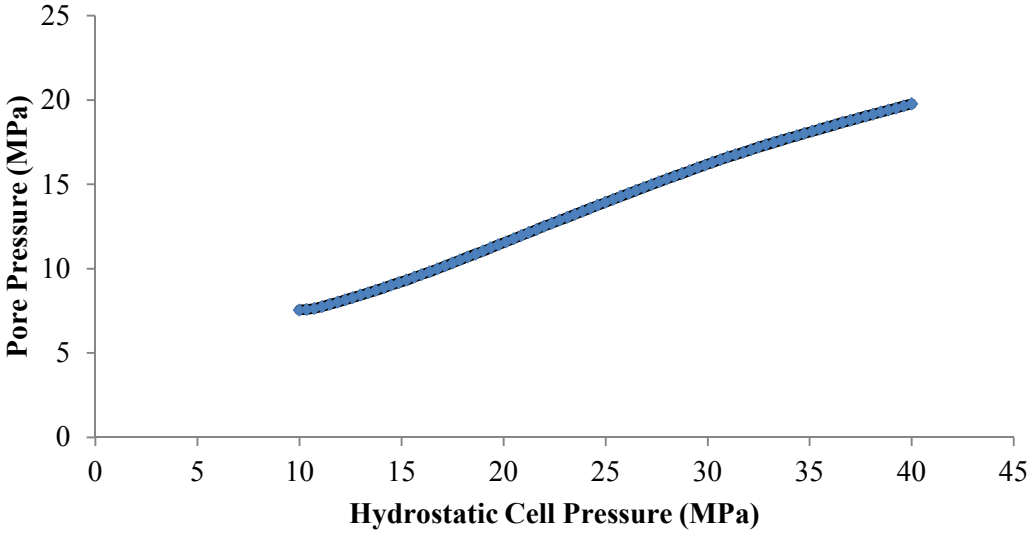

Figure 22: Hydrostatic Undrained test for specimen N1-4013-3H.

Figure 22 shows the pore pressure response of rock specimen N1-4013-3H in hydrostatic undrained conditions. As opposed to specimens N1-4348-1V and N2-4281-4V, the pore pressure changed in a uniform manner along the duration of the test. This might happen because this specimen has a well sorted size distribution and no noticeable fractures, if compared to the two previous. By having a uniform size distribution, the fluid would distribute evenly within the rock during the saturation process leading to a uniform pore pressure response during the test.

The data obtained from the hydrostatic undrained test was used to determine the Skempton's pore pressure hydrostatic parameter B for the three welded tuff core samples. In Figure 23 is interpreted the value of parameter B at different confining pressures for the rock specimen N1-4348-1V. The parameter B grew with a parabolic tendency from a value 0 to 0.26 in the interval between the beginning of the test and 27 MPa, to then reach its peak value in the interval of 27 MPa until the end of the test. The maximum value of the B parameter calculated was 0.28. The specimen N2-4281-4V presented a peak value for B of 0.33 at 12 MPa and a maximum value for B of 0.49 at a confining stress of 22 MPa, as can be observed in Figure 24. For the last specimen labeled N1-4013-3H the maximum peak for the parameter B was observed at 29 MPa with a calculated value of 0.49 (See Figure 25). While for the specimen N1-4348-1V the calculated B value increases until reaching and keeping its maximum value, for the rock samples N2-4281-4V and N1-4013-3H the B value decreased after reaching its peak.

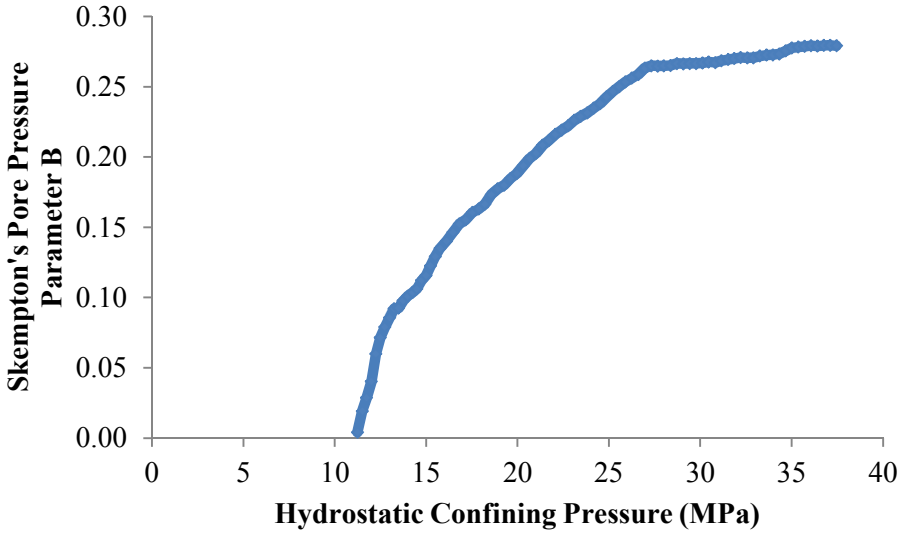

Figure 23: Skempton's pore pressure parameter B for N1-4348-1V.

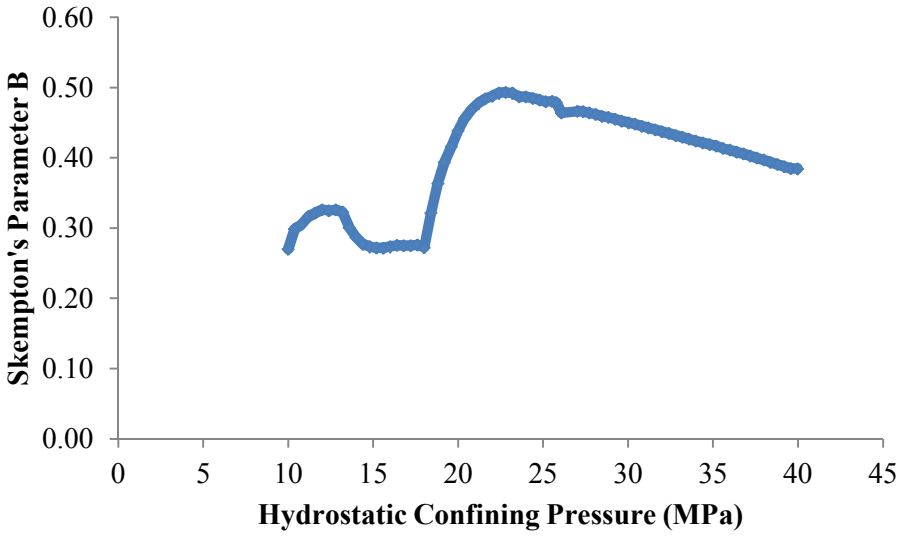

Figure 24: B values for specimen N2-4281-4V.

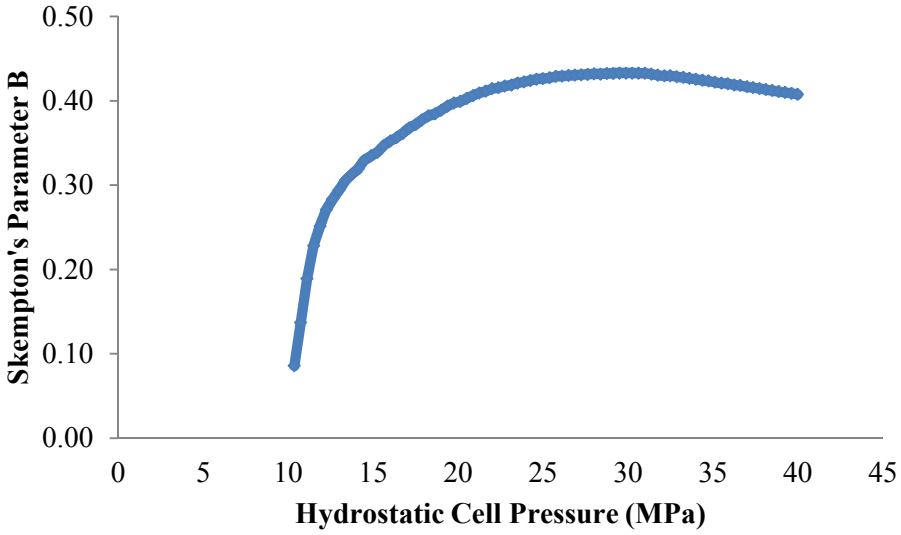

Figure 25: Skempton's B values for N1-4013-3H.

To summarize, Table 3 shows the B values obtained from the undrained experiments performed to the specimens labeled N1-4348-1V, N2-4281-4V and N1-4013-3H, along with their correspondent permeabilities and porosities.

Table 3: Petrophysical properties of the Welded Tuff rock specimens.

Specimen ID	Porosity	Permeability (md)	B value
N1-4348-IV	12.38% to 16.71%	1.17e-2 to 5.21e-2	0.28
N2-4281-4V	4.9% to 6.44%	7.40e-05	0.49
N1-4013-3H	1.79% to 3.35%	1.68e-4 to 6e-4	0.43

From this table it can be observed that the lowest pore pressure response to the load applied occurred with specimen N1-4348-1V, while the response was higher with the other two specimens. It can be observed that the specimen N1-4348-1V also has a

very noticeable higher porosity and the higher permeability if compared to the other two specimens. After analyzing the petrographic thin sections as stacked images we noticed that this rock specimen had a mechanical fracture caused by axial compression before our experimental procedures. In this non-homogeneous rock by having a substantially higher porosity and permeability, the fluid is allowed to displace through the rock fractures easier than in the other two cases. If the volume of fluid stored in the fracture is large and the fluid redistributed with less constraints, then the pore pressure buildup caused by the increasing confining stress would be smaller. Therefore, the porosity, permeability and B value for specimen N1-4348-1V presented in Table 3 are not representative of the rock, but of the fracture system within the rock.

6.2 Determination of Biot's Coefficient of Effective Stress, α

Biot's coefficient of effective stress α can be calculated by using an experimental indirect method proposed by Geertsma and Skempton:

$$\alpha = 1 - \frac{K}{K_s}$$

where K is the Bulk Modulus and K_s is the compressibility of the grain. The compressibility of the grain is obtained by calculating the slope the hydrostatic stress versus volumetric strain curve, during the unjacketed test. In this indirect method a set of two experiments are needed to estimate the parameter α, namely an unjacketed hydrostatic test and a jacketed hydrostatic drained test. The unjacketed test is used to determine the compressibility of the grain matrix, while the jacketed test will estimate the compressibility of the rock matrix.

For the unjacketed test, the rock specimen is placed in the triaxial cell and then saturated for 24 hours at a pressure of 6.89 MPa using an external hydraulic pump, which contains the same fluid as the confining fluid for the triaxial cell Paratherm NF that is a non-toxic white mineral oil that is rated for food and pharmaceutical use. After rock specimen was fully saturated, the pressure was decreased to 7 MPa to initialize the test. During the hydrostatic test, the specimen was loaded at a constant rate of 0.5 MPa/min until the confining pressure reached a value of 40 MPa.

The results obtained through the drained and unjacketed test are summarized in Table 4. The following pages discuss in detail each experimental procedure and present the plots for each performed test.

Table 4: Calculated values for Biot's coefficient of effective stress in Welded Tuff.

Specimen ID	K (GPa)	Ks (GPa)	α
N1-4348-IV	2.33	55.49	0.95
N2-4281-4V	27.32	51.26-78.06	0.47-0.65
N1-4013-3H	33.45	45.97-73.86	0.27-0.55

6.2.1 Drained Test

It was determine by the first round of experiments that the fluid withdrawal method was not accurate enough to determine Biot's coefficient α. A new set of experiments was performed in which the drained test was only used for determining the Bulk Modulus of the rock, K. The drained test was performed in the Rock Triaxial

System RTX-1500, while the pore fluid was provided using the syringe pump ISCO 100 DM. The rock specimen was saturated into the pore fluid for 24 hours using the mineral oil Paratherm NF at room conditions, prior to the test. Paratherm NF was selected for this experiment because we found it to have very low compressibility (0.335/GPa) if compared to water that is usually used as pore fluid (2.75/GPa). For these experiments a hydrostatic confining pressure of 10 MPa was applied to the rock specimen while the pore fluid was injected at a rate of 0.5 MPa/min, until a pore pressure of 6.89 MPa was reached. After the goal pore pressure was achieved, the strains and the pump flow rate were monitored until a state of equilibrium of the fluid was found. We assumed that the equilibrium was met when the flow from the syringe pump started displacing back to the pump, meaning that not anymore flow is allowed into the rock because it is fully saturated and in order to keep the current state of stress. When the axial and circumferential strains became constant after the goal pore pressure was reached, the specimen was considered to be fully saturated because no more fluid is allowed to flow into the sample. When the fluid was injected into the rock in order to increase the pore pressure to a value a 6.89 MPa, it was shrinking because the pore fluid was being injected at a faster rate than the fluid entry value, resulting as a concentration of stresses in the surface of the rock that caused an increment of effective stresses, causing deformation of the specimen.

When the rock was fully saturated, then the pore pressure was stabilized, the effective stress value was reduced and the rock specimen was not deforming. By using experimental methods we obtained the Bulk Modulus of Berea Sandstone (10.13 GPa),

Indiana Limestone (14.28 GPa) and Westerly Granite (16.24 GPa) as preliminary testing.

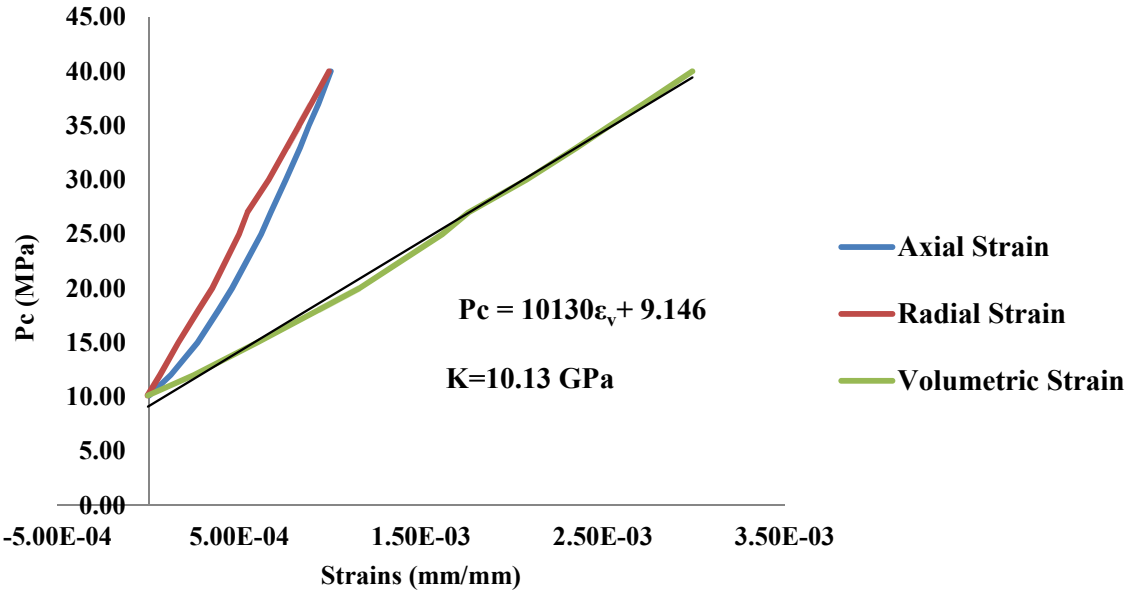

Figure 26: Bulk Modulus calculation for Berea Sandstone.

For Berea Sandstone, it was observed that the rock specimen was fully saturated before the set time of 24 hours, but it was left for the 24 hours in order to simulate the same laboratory conditions for the all of the specimens.

As can be observed in Figure 26, the rock specimen was loaded from an initial hydrostatic confining pressure of 10 MPa to a final constant pressure of 40 MPa while the pore pressure was constant along the whole duration of the test, at a value of 6.89 MPa. For the duration of the test, the rock specimen remained within the elastic range of

deformation. The high porosity of the specimen and the homogeneity of the grains allow a great amount of deformation in the elastic range prior to the collapse of the pores. The homogeneity and isotropy of the rock might be the reason for having very similar axial and circumferential strains.

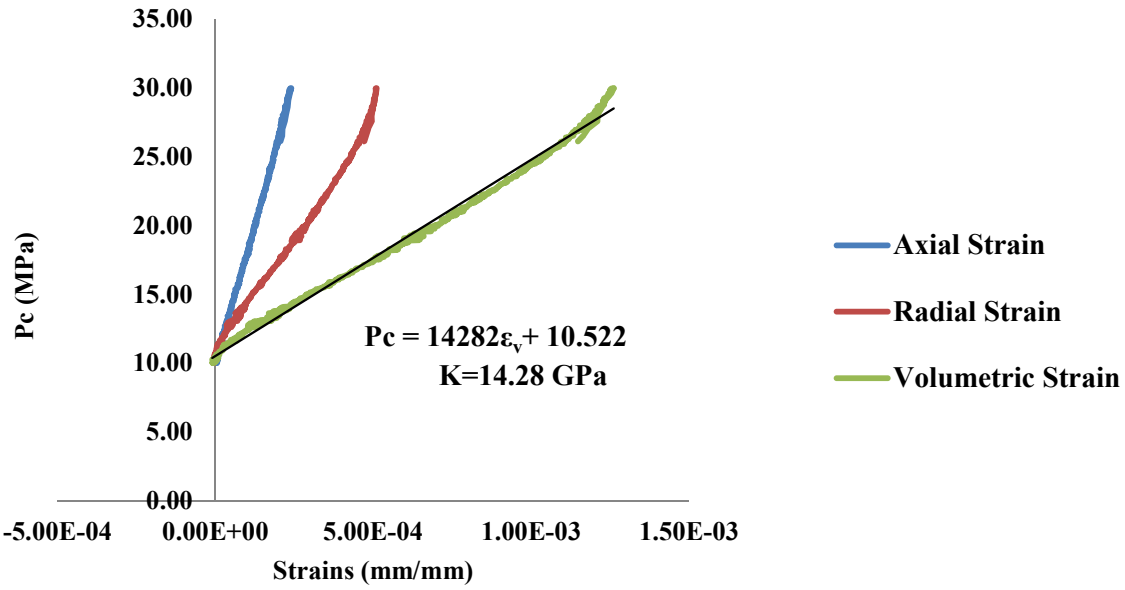

Figure 27: Bulk Modulus plot for Indiana Limestone.

For Indiana Limestone (Figure 27) the test was stopped at 30 MPa because components such as tubing fittings were replaced and in order to ensure the safety of the equipment, the test was stopped under the minimum nominal pressure rating for all the components. In this test the radial strain was approximately half of the axial strain, which might be caused by the mineralogy of the rock. It can be observed that there are

more data points for this experiment if compared to the Berea sandstone, but it was because we changed the monitoring to every second for this and the coming tests. The loading rate was kept at 0.50 MPa/min during the duration of the test. The rock was considered as fully saturated when the flowing rate of the pore fluid only fluctuated between ± 0.004 mL/min. When the pore pressure in the bottom platen only dropped less than the 2% of the pore pressure (0.27 MPa) when the ball valve installed between the pore fluid source pump and the system was closed, was an indicative that the rock was fully saturated.

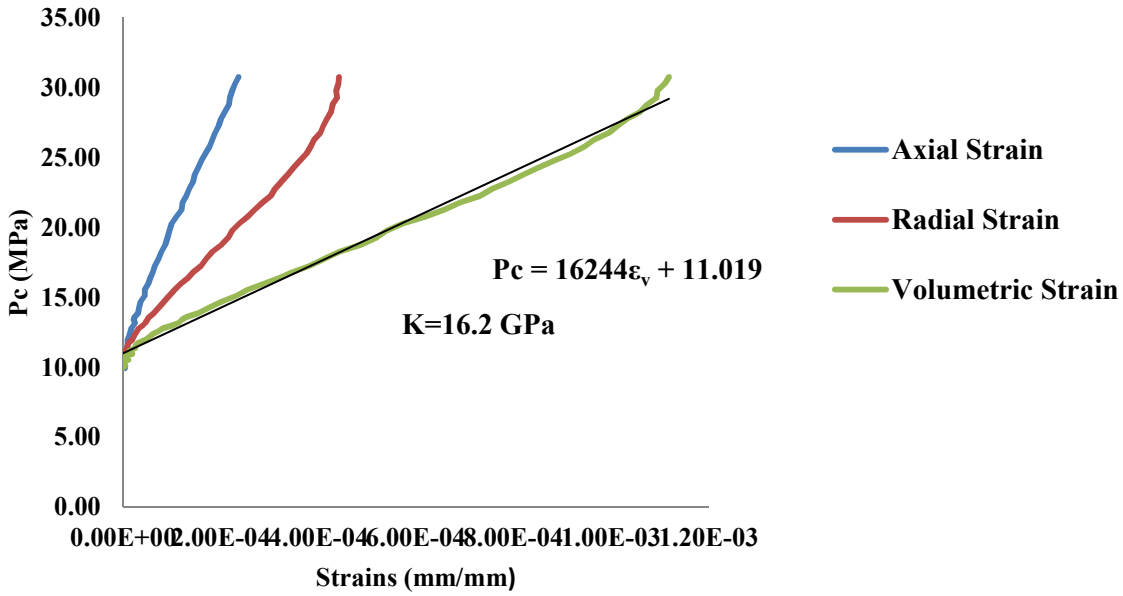

Figure 28: Bulk Modulus for Westerly Granite.

In Figure 28 we can observe the drained test performed for Westerly Granite. This rock specimen took about 24 hours to saturate because of the low connectivity between the pores and its low permeability. The same loading and saturation given to

Indiana Limestone was provided for the Westerly Granite. During the beginning of the test the deformations were very small because the deformations might not be noticeable at these stress levels. During the elastic region of the deformation plot an almost linear volumetric deformation that gave as a result a bulk modulus of 16.2 GPa was observed. As the stress level increases the bulk modulus increases and the evidence is that the slope of the stress-strain curve gets steeper at the end of the test. This might be because when the specimen is loaded the porosity get reduced at the point that the minerals and the cements contained in this rock at supporting all the load applied, giving it mayor strength if compared to the case that the pore fluid is carrying part of the load.

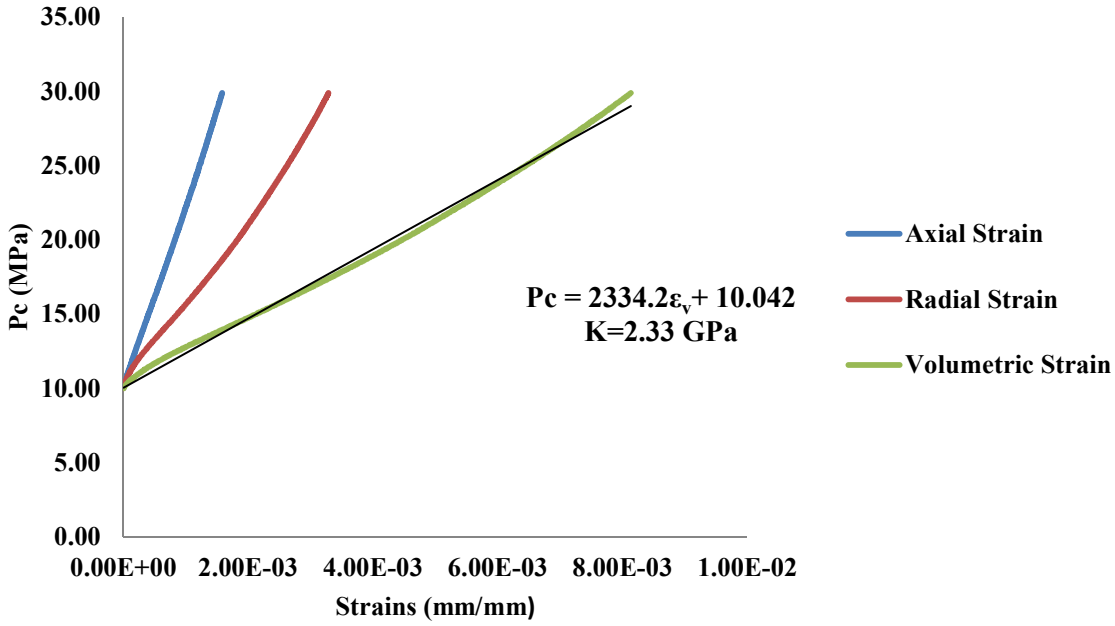

Figure 29: Bulk Modulus for Welded tuff N1-4348-1V.

For the Welded Tuff N1-4348-1V the saturation procedure resulted very similar as for the Westerly Granite in duration and behavior. As in the previous tests, the rock specimen was loaded hydrostatically up to a confining pressure of 30 MPa, with a constant pore pressure of 6.89 MPa. From the Figure 29 we can observe that the circumferential strain is larger than the axial strain and this might be because this rock has a highly heterogeneous particle distribution. This core was also drilled vertically and the overburden vertical stresses provide the rock with additional vertical strength due to the stress history, resulting in overconsolidated specimen if it loaded hydrostatically, leading to small deformations in the axial direction. This test gave as an outcome a Bulk Modulus of 2.33 GPa, which indicates that this pyroclastic rock is highly compressible. The high compressibility of this core might be because it has a significantly measured high porosity (14.60%), and because it is mostly composed the specimen can be described as fine grained and well sorted.

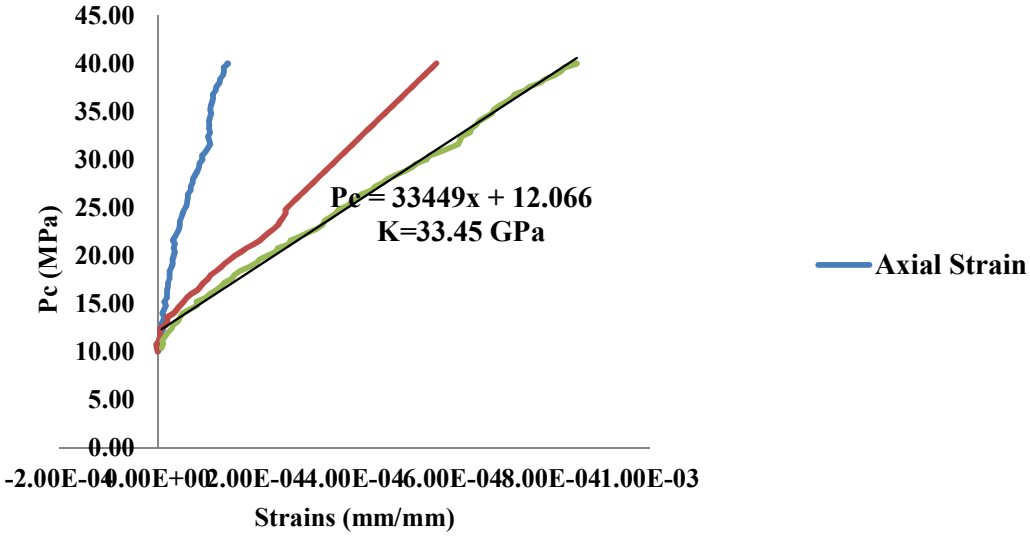

Figure 30: Bulk compressibility for Welded Tuff N1-4013-3H.

In Figure 30 we observed the test performed for measuring the bulk compressibility in the Welded tuff specimen labeled N1-4013-3H. For this test, the specimen was loaded hydrostatically from 10 MPa up to 40 MPa, at a constant rate of 0.5 MPa/min. After the test was finished, the bulk modulus for the specimen was calculated to be 33.45 GPa, higher than for the previous sample N1-4348-1V, due to their different composition and alignment of the minerals that might affect their mechanicals properties.

6.2.2 Unjacketed Test

The Unjacketed Test was performed by installing two axial LVDTs and one chain gauge holding the circumferential LVDT, both installed directly into the rock specimen, as can be observed in Figure 32. For an unjacketed test, the pore pressure must equal the cell pressure so that the grains are subjected to a net pressure. It is therefore essential to have the sample fully saturated. For this case, the sample is installed and the cell filled with oil and the absence of an impermeable phase between the rock specimen and the oil in cell allows the migration of the oil into the pore space (See Figure 31).

The dry rock was saturated within the filled cell with Paratherm NF® as a confining fluid, for a period of 24 hours, using a cell pressure of 6.89 MPa. This was achieved by filling up the triaxial cell with mineral oil and pressuring the cell using a syringe pump, and making sure that the syringe pump is free of entrapped air by opening the other outlet in the syringe pump until oil started flowing continuously and then closing it inmediately. The entrapped air causes the pump to refill only with pore fluid partially; therefore the availability of pore fluid is reduced in half, if the previous procedure is not followed. After the strains in the rock remain unchanged and the rock is fully saturated, the cell pressure is increased at a rate of 0.33 MPa/min. The loading rate was selected by taking into consideration the testing ASTM D 5407 – 95, which standardize the test method for Elastic Moduli without Pore Pressure Measurement. This standard explains that a loading rate can be selected as long as it is kept constant or do not differ in 10% of the selected rate during the loading process. To verify this

statement, pre-loading stages were performed at different loading rates, and it was observed that within a range of 0.33 MPa/min to 0.8 MPa/min the loading rate was not affecting the grain compressibility obtained from the unjacketed tests.

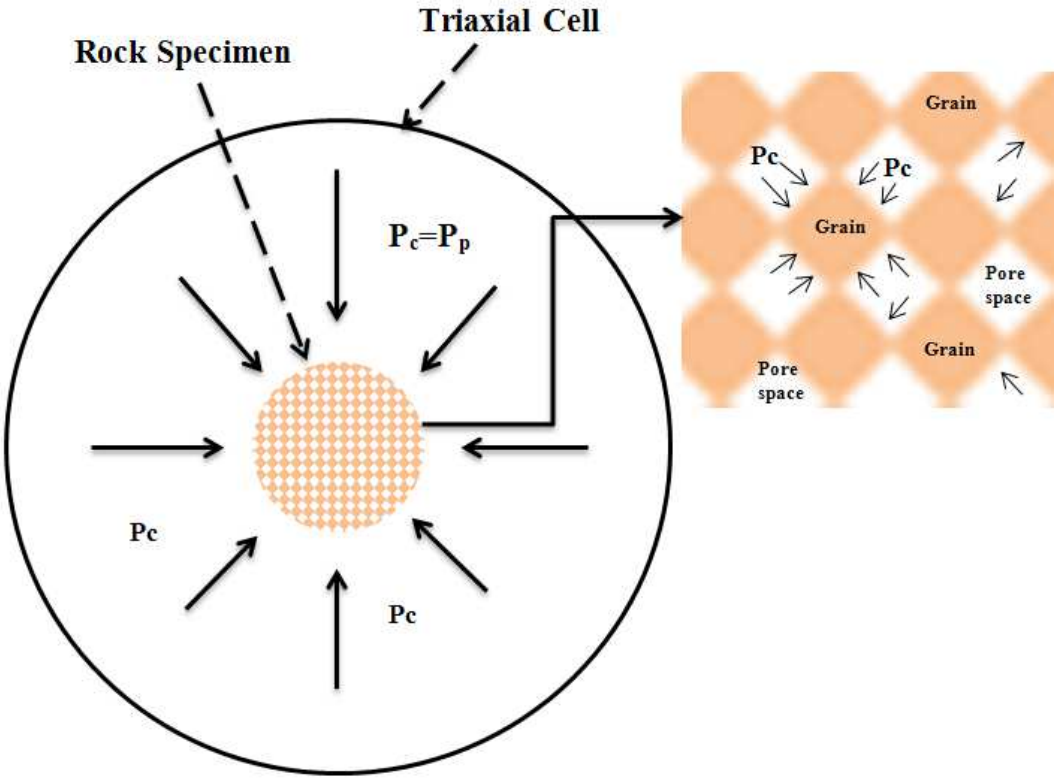

Figure 31: Grain compressibility diagram.

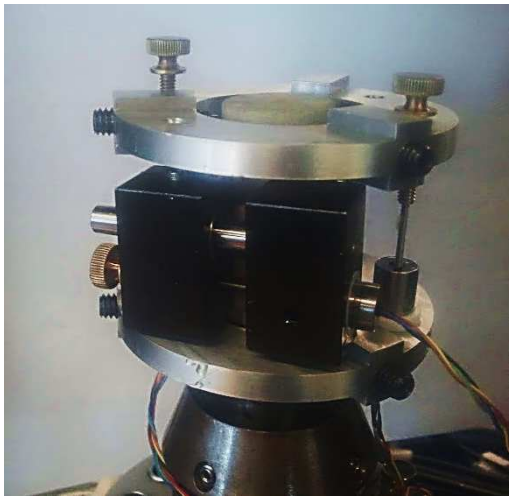

Figure 32: Experimental Setup for the unjacketed test.

The grain compressibility K_s can then be calculated in a manner similar to that for the bulk modulus K. The grain compressibility for Berea Sandstone is 34.2 GPa (Figure 33), for Indiana Limestone 74.69 GPa (Figure 34), for Westerly Granite 48.01 GPa (Figure 35), for Welded Tuff N1-4348-1V is 55.6 GPa (Figure 36), for specimen N2-4281-4V the value ranges from 51.26 GPa to 78.06 GPa, while for rock specimen N1-4013-3H the grain compressibility varied from 45.97 GPa to 73.86 GPa.

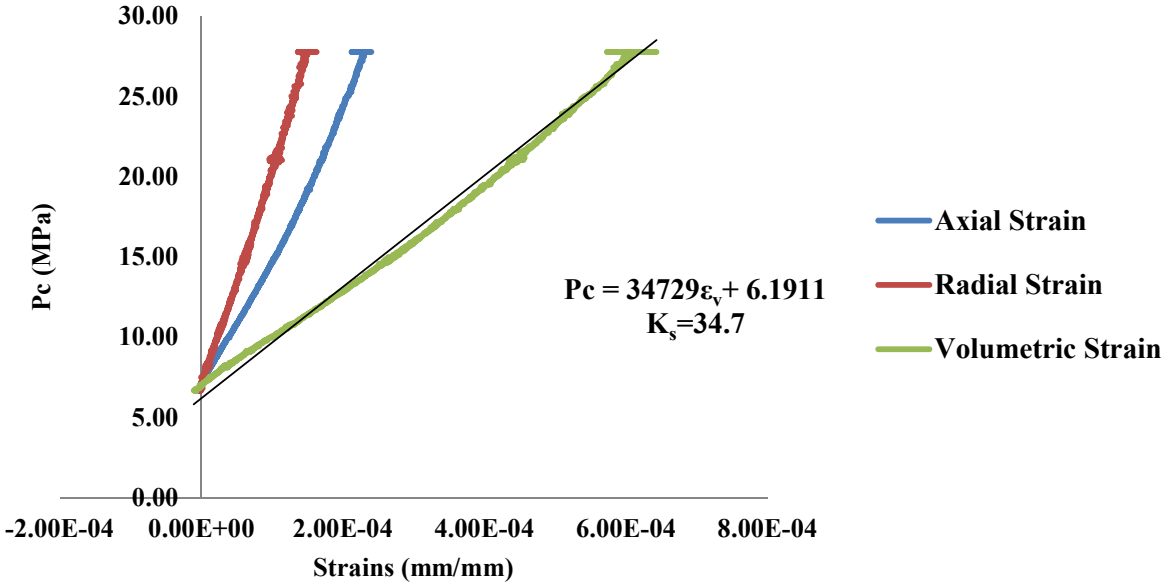

Figure 33: Unjacketed hydrostatic compression test for Berea Sandstone.

The Berea Sandstone labeled B-S-7 was fully saturated within the first hours, but it was left pressurized for the 24 hours at 6.89 MPa as it was previously established for all the rock cores object of our study.

For this test on Berea Sandstone, the radial strain are smaller than the axial strain as displayed in Figure 33, if we compared it to the drained test where both of them were almost equal. The compressibility of the grain obtained is 34.7 GPa for this specimen.

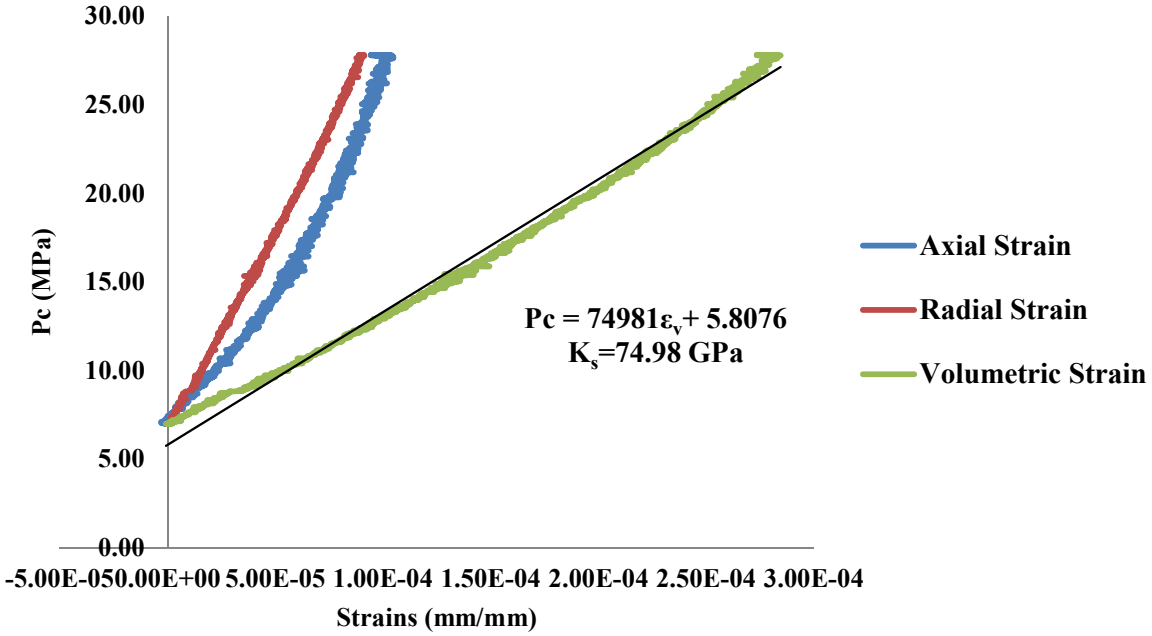

Figure 34: Unjacketed hydrostatic compression test for Indiana Limestone.

Figure 34 shows the unjacketed test for Indiana Limestone. The specimen was saturated in less than 24 hours, but as discussed above, it was left for 24 hours to have a standard procedure for all the specimens. The test was started at a confining pressure of 6.89 MPa and was terminated at 28 MPa, at a loading rate of 0.33 MPA/min. In this case the axial strain is almost equal to the radial strain during loading. It can also be observed that the slopes of the plots are increasing with the stress applied, meaning that the grain compressibility gets reduced at higher levels of stress because the grain particles are reaching their maximum deformation prior to collapsing or by the closure of dead pores and cracks. An approximate linear slope was draw in order to obtain the grain

compressibility, and the value of the grain compressibility obtained was 74.98 MPa. This is a very large grain compressibility modulus, meaning that the major contributor of the bulk rock compressibility is the pore space of the rock, rather than the grains itself.

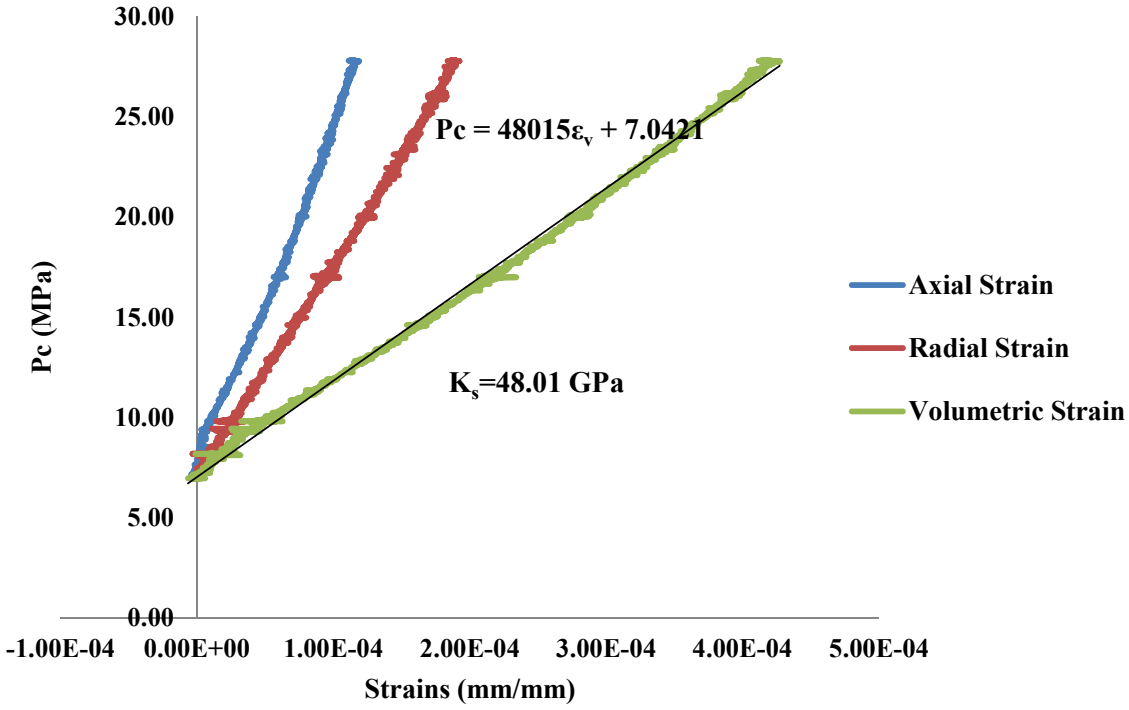

Figure 35: Grain compressibility for Westerly Granite.

The Westerly Granite grain compressibility was obtained from the test displayed in Figure 35. The saturation process took 24 hours plus two more hours to verify that there were not strains still going in the rock because of the injection process. The compressibility of the grain behaves very linear when compared to the bulk compressibility of this rock. During the unjacketed test all connected pore spaces are

filled with the confining fluid and therefore all the grains are allowed to deform evenly, without the change of the volume attributed to the change in the pore space. For the Westerly Granite the grain compressibility modulus is 48.01 GPa, or three times greater than its bulk compressibility, meaning that most the deformation attributed to this type of rock is caused the pore space.

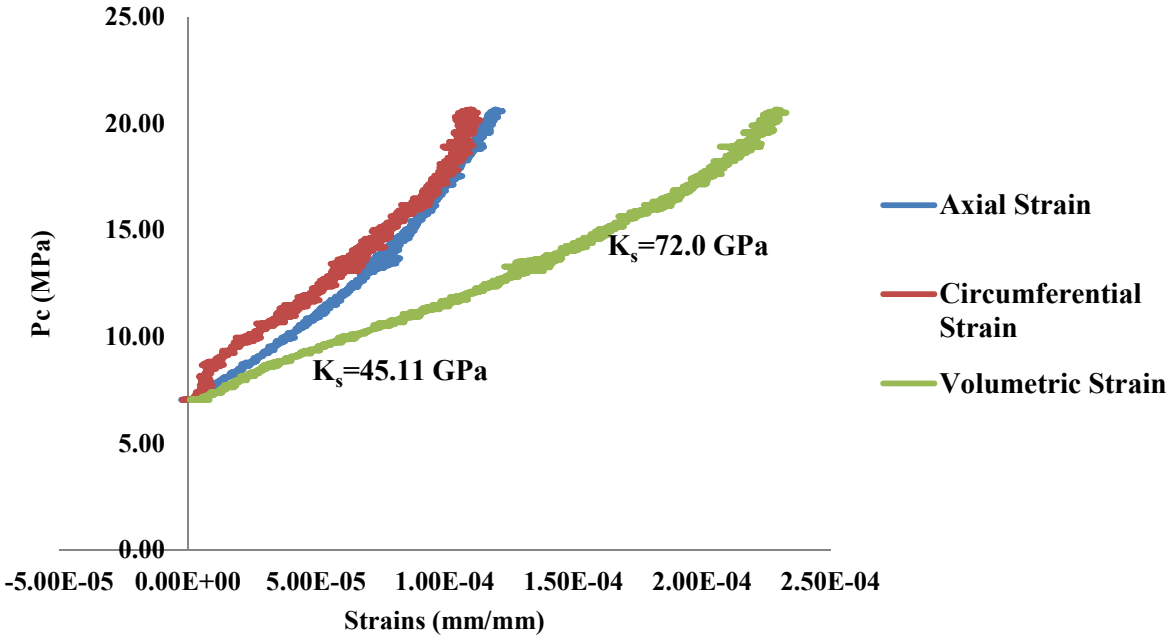

Figure 36: Grain compressibility for Welded Tuff N1-4348-1V.

In Figure 36 it can be observed the unjacketed test performed for the Welded Tuff, sample N1-4348-1V.

As for the Westerly Granite, the saturation took the around 24 hours in addition to 2 hours after the saturation to verify that the specimen was not deforming because of

the pore fluid entering or leaving it. For the Welded Tuff, the deformations were higher at the beginning of the test and during the progress of the test the stress-strain curve got steeper meaning that at higher pressures the grain is less likely to deform, prior the reaching its maximum deformation, due to the changing compaction mechanism during the loading process. The radical slope change observed after ~ 18 MPa might be caused by strengthening in the grain product of the closure of fissures produced during the grain collapse. For the first part of the experiment the average grain modulus calculated is 45.11 GPa and for the second part of the experiment, the calculated grain modulus is approximately 72.0 GPa.

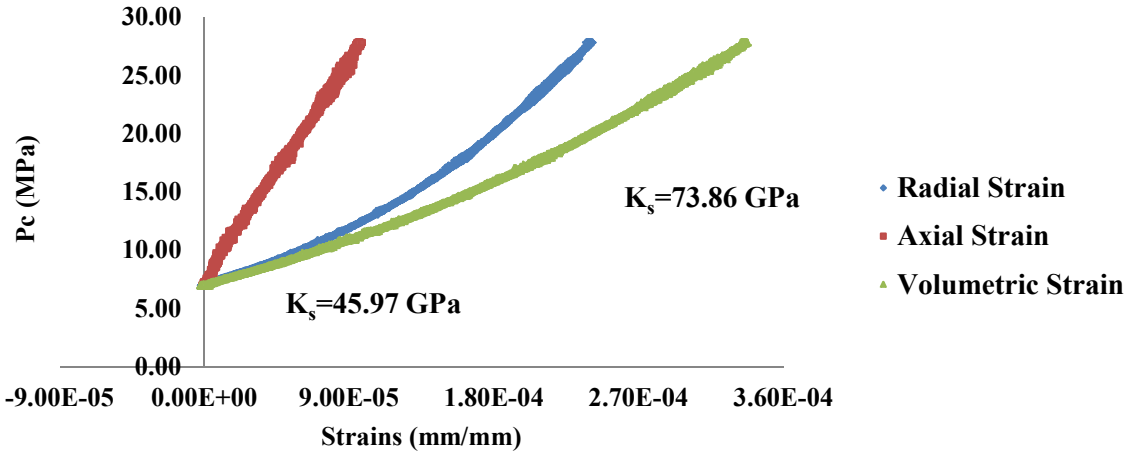

Figure 37: Grain compressibility for specimen N1-4013-3H.

After fully saturated, the Welded Tuff specimen N1-4013-3H (Figure 37) was loaded from a value of approximately 6.9 MPa (1 000 psi) up to approximately 27.5

MPa (4 000 psi), at the same constant loading rate as in the previous experiments. In order to obtain the grain compressibility for this specimen, the slope was separated into two parts and then the grain compressibility K_s was calculated to be a value of 45.97 GPa at hydrostatic pressures of 6.9 MPa to approximately 73.86 GPa from 15 MPa of hydrostatic pressure, up to the end of the experiment. As the confining pressures were getting higher, the solid started to present more resistance to deformation because it was transitioning from elastic state of deformation to non-elastic deformation.

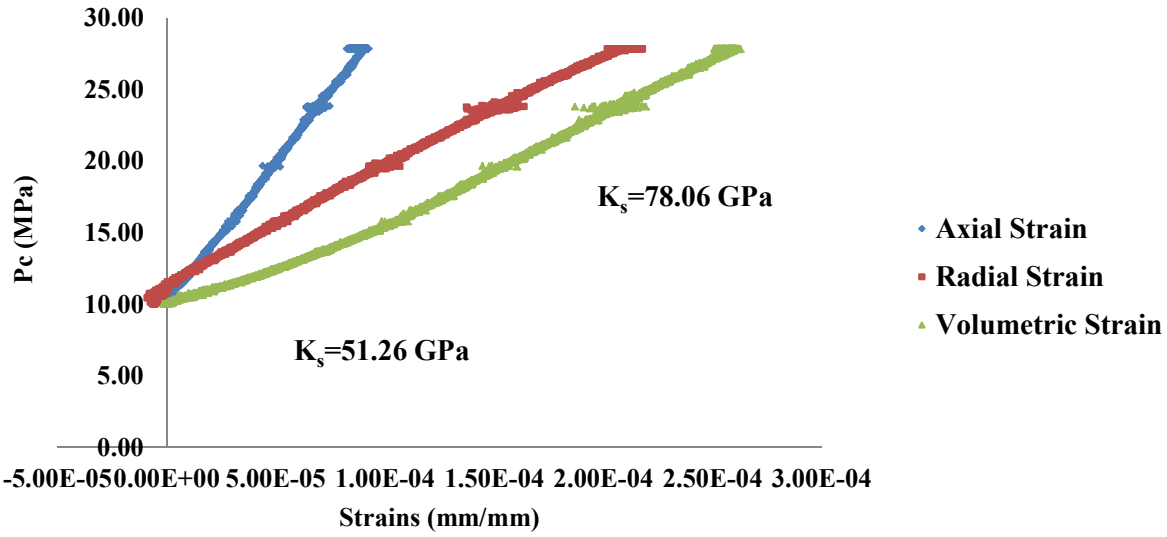

Figure 38: Grain compressibility for specimen N2-4281-4V.

In the rock specimen N2-4281-4V, the pattern for the compressibility was different to specimens N1-4348-1V and N1-4013-3H. This current specimen was recover from corehole Geo N-2, located 9 Km NW of corehole Geo N-1, which is the

source for specimens N1-4348-1V and N1-4013-3H in the Newberry Volcano in Oregon (See Figure 3). The specimens obtained from site Geo N-1 present smaller lateral deformations, while the opposite happened to the specimen from site Geo N-2 where the axial strain is noticeable smaller than the radial strain. For this case the grain compressibility was obtained from calculating two different slopes of the confining pressure with respect to the volumetric strain. The average grain compressibility obtained was 64.66 GPa. From a confining stress of 10.0 MPa to 16.0 MPa the grain compressibility calculated was 51.26 GPa and from 16.0 MPa to 27.0 MPa the value was 78.06 GPa. It can be noted that for both specimens, the grain compressibility modulus increased in approximately 50% ~ 60% for the second part of the curve.

6.3 Results Accuracy

In order to verify the results obtained from our experimental procedure, the compressibility obtained from our drained and unjacketed tests in the Berea Sandstone were compared to the values obtained by other authors. The comparison is made in Table 5. Further analysis will be carry out in the next step of this project to estimate a metric of comparison for the specimens without enough data, by analyzing the individual properties of the particles contained in the rock.

Due to the lack of information in the literature for the Welded Tuff, the bulk compressibility was calculated by using the equation below, which comes from the derivation of Hooke's Law:

$$K = \frac{E}{2\,(1 - 2\,\upsilon)}$$

This information was obtained from the multistage test presented in the next section. In order to obtain the poisson's ratio υ and the Young's Modulus E, the stress-strain relations of the general Hooke's law for isotropic linear elastic cylindrical material were used as displayed in Figure 39 :

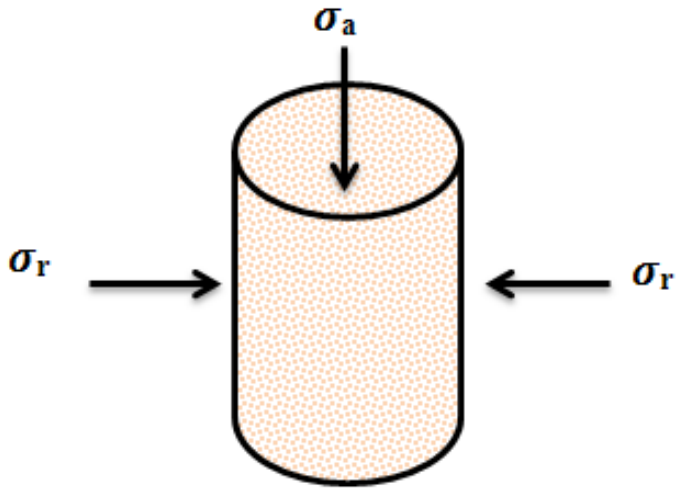

Figure 39: Stress-strain diagram for 3-D Hooke's Law.

$$\sigma_a = \frac{E}{(1+\upsilon)(1-2\upsilon)}[(1-\upsilon)\varepsilon_a + \upsilon(2\varepsilon_r)]$$

(1)

$$\sigma_r = \frac{E}{(1+\upsilon)(1-2\upsilon)}[(1-\upsilon)\varepsilon_r + \upsilon(\varepsilon_a + \varepsilon_r)]$$

(2)

By combining (1) and (2) we obtained that the poisson's ratio can be calculated as

$$\upsilon = \frac{(\sigma_a \varepsilon_r - \sigma_r \varepsilon_a)}{(2\,\sigma_r \varepsilon_r - \sigma_r \varepsilon_a - \sigma_a \varepsilon_a)}$$

(3)

And then after we can obtain the Young's modulus E by using either (1) or (2). The results of the calculations of the elastic parameters are displayed in Table 5. It can be observed that the values for the Poisson's ratio obtained from the linear elasticity theory using the strains obtained are within the range of values previously observed in other experiments.

In order to verify the results from our drained experiments in reference to the Bulk modulus of the rock, our results for the two specimens obtained from corehole GEO N1were compared to calculations obtained from multistage triaxial stages in Newberry Tuff (Li, et al, 2012). The values of the Poisson's ratio and of the Young's modulus were used to calculate an estimated K in order to compare with our experimental results, as described in the equation below:

$$K = \frac{E}{3(1 - 2\nu)}$$

For the core N1-4013 the bulk modulus K obtained was 27.2 GPa and for the core N1-4348 K value was 16.6 GPa. For the recovered core N1-4348-1V we can observe from Table 6 that our obtained value for K is substantially lower than the referenced value, but it is because our specimen presented a mechanical compressional

fracture, meaning that the fracture is open and will at a very low stress level because is not propped, and the bulk deformation would be higher, giving a low bulk modulus.

Table 5: Calculated elastic properties of Berea Sandstone.

Stage from the Multistage test	Pc (MPa)	ν	K (GPa)	E (Gpa)
1	3.44	0.26	8.68	9.21
2	6.89	0.28	15.59	17.60
3	10.31	0.31	16.11	20.74
4	17.19	0.34	18.88	29.38
5	24.06	0.35	20.28	33.25

Table 6: Calculation of Biot's Coefficient α.

Rock ID	K (GPa)		K_s (GPa)		α		Author (s)	Method used by compared author(s)
	This work	Other authors	This work	Other authors	This work	Other authors		
Berea SS	10.13	4.0-12.5/ 0.95	34.72	47.2/ 29.8	0.71	0.8	Richin/ Herbert and Wang	Indirect Method
India-na LS	14.28	20.83	74.9	76.9	0.81	0.84	Richin	Indirect Method
Westerly Granite	16.24	15-25	48.01	N/A	0.66	0.60	New England Research	Uniaxial Strain and dynamic measurements
Welded Tuff N1-4348-1V	2.33	16.6	45.11/ 72.00	43.6/ 79.3	0.96	0.62/ 0.79	Voigt and Reuss/ Li	*Mineral volume weighted average
Welded Tuff N2-4281-4V	27.32	N/A	51.26/78.06	37.2/ 85.1	0.47/ 0.65	N/A		
Welded Tuff N1-4013-3H	33.45	27.2	45.97/73.86	43.6/ 79.3	0.27/ 0.55	0.37/ 0.66		

It can be observed from Table 6 that the values of the bulk modulus, grain compressibility and α for Berea sandstone, Indiana limestone and Westerly granite are very similar to values obtained in other experiments performed by other authors using indirect experimental methods, as we did in order to calculate Biot's coefficient of effective stress α.

In order to verify the compressibility values for the Welded tuff specimens, a weighted average method was used to approximate the properties of the composing minerals to the properties of the rock bulk. For this purpose, the fundamental spatial averaging models developed by Voigt (1910) and Reuss (1926) based on sheet models were used in which averaging schemes to estimate the elastic constants in monomineral aggregates (Kobranova, 1986). This theory assumes that the aggregate could behave isotropically if there is no preferred orientation of mineral grains and their crystallographic axes. For the application in heterogeneous rocks, this model assumes that the individual rock components (minerals and cementing material) are separated and arranged in a sequence of sheets. In this theory the relative thickness of the individual sheet is proportional to the volume or weight fraction of each component and its corresponding properties. The two models represent macroscopic homogeneity: Voigt moduli represent homogeneous strain and the Reuss moduli represent homogeneous stress. The Voigt modulus is calculated as described below, where the index i refer to each component, while k_i refers to the bulk modulus and V_i refers to the volume fraction of each component.

$$K_V = \sum_{i=1}^{n} k_i V_i$$

In the same way, the Reuss bulk modulus is calculated by arranging the mineral properties in parallel:

$$\frac{1}{K_R} = \sum_{i=1}^{n} \frac{V_i}{k_i}$$

The Voigt modulus calculation will determine the upper limit of the grain bulk modulus, while the Reuss relationship the lower bound. The real values are located anywhere between these two limits. For our purposes, the mineral composition by weight percentage was approximated by using the data from coreholes Geo N1 and Geo N2 (Bargar, 1999) at different depths (see Table 7 and Table 8). With the help of the Palisade® decision tool @Risk, a quantitative analysis of the mineralogy with depth was performed to estimate the properties of the core plugs used for this experiment. After observing that the mineralogy is not correlated with depth, we fitted the minerals weight percentage to data distributions and generated random iterations within the distribution in order to calculate the median, which was used as the weighted average value for the calculation of Reuss and Voigt modulus (Anderson, 1965) and (Bakhorji, 2010).

Table 7: Mineralogical composition for corehole Geo N1.

Mineralogical component	Weight percentage (%)	Bulk Modulus (GPa)
SiO_2	50.86	36
Al_2O_3	29.69	165
FeO	0.59	178
MgO	0.10	150
CaO	13.55	111
K_2O	0.078	54
Na_2O	3.72	11.6
SrO	0.18	216
	K_V=	**84.37**
	K_R=	**49.01**

Table 8: Mineralogical composition for Geo N2.

Mineralogical component	Weight percentage (%)	Bulk Modulus (GPa)
SiO_2	55.05	37.1
Al_2O_3	15.53	228
Fe_2O_3	7.65	178
MgO	2.40	150
CaO	4.87	111
Na_2O	3.75	61.1
K_2O	1.41	11.6
TiO_2	1.33	216
P_2O_5	0.34	35.1
MnO	0.16	143
H_20	3.66	23.7
CO_2	1.99	3.0
Cl	0.15	11.7
S	0.05	17.3
	K_V=	**85.05**
	K_R=	**37.21**

After calculating the Voigt and Reuss modulus, it was easily detected that the values for grain compressibility were within the expected upper and lower bounds of compressibility, which validate our experiments. Although there is no available data for coefficient α for this rock, it is inferred that the value can be obtained by using the compressibilities obtained above. During the unjacketed hydrostatic tests in Tuff, it was observed that from 6.9 MPa to approximately 15.0 MPa the grain is more compressible (lower K_s) and from 15.0 MPa to 30.0 MPa the compressibility of the grain starts to decrease (higher K_s). It was observed that the grain compressibility at different stress levels can be described with the help of Voigt and Reuss' models. With these models, it was determined that at lower stress levels the stress distribution is uniform in accordance with the Reuss model, while at larger stress levels it behaves in accordance with the Voigt approach of uniform strains. It was demonstrated that the changes in matrix compressibility should be taken into consideration to calculate Biot's coefficient of effective stress α and that Ks behaves in compliance with Voigt and Reuss' models depending on the stress level.

6.4 Effects of the Saturating Phase in the Rock Properties

6.4.1 Multistage Experiment in Berea Sandstone

After the poroelastic tests were completed, multistage triaxial tests were performed in a triaxial rock specimen (Berea Sandstone) in order to determine how the mineral oil might affect the mechanical properties of the rock. The multistage triaxial test was not performed in the other specimens in order to avoid using them for a

destructive test. For Berea sandstone, a 5 stage multistage test was performed under the confining stresses of 3.44 MPa, 6.89 MPa, 10.31 MPa, 17.19 MPa and 24.06 MPa as displayed in Figure 40, Figure 41, Figure 42, Figure 43 and Figure 44 respectively. The strain rate used for all the stages was 1 x 10^{-6} mm/mm/s. The angle of internal friction was calculated by drawing a tangent to all the circles, and the Mohr-Coulomb failure envelope was used to determine it. From this test we can observe that for this rock the angle of internal was larger (43°), if compared from a compression typical case when it is about 31°-33° (Aristotelis, 1994) for a multistage test. It can also be inferred that a larger angle of internal friction should be expected because we could observe that the ultimate load is larger when the mineral oil is the saturating phase. The smaller angle of internal friction observed when water was used as the wetting phase, is as a cause of the weakening caused in the rock by the water. Using triaxial tests at different confining pressures, Hadizadeh and Law (1991) showed evidence of the water weakening in sandstones and quartzite when stresses were applied.

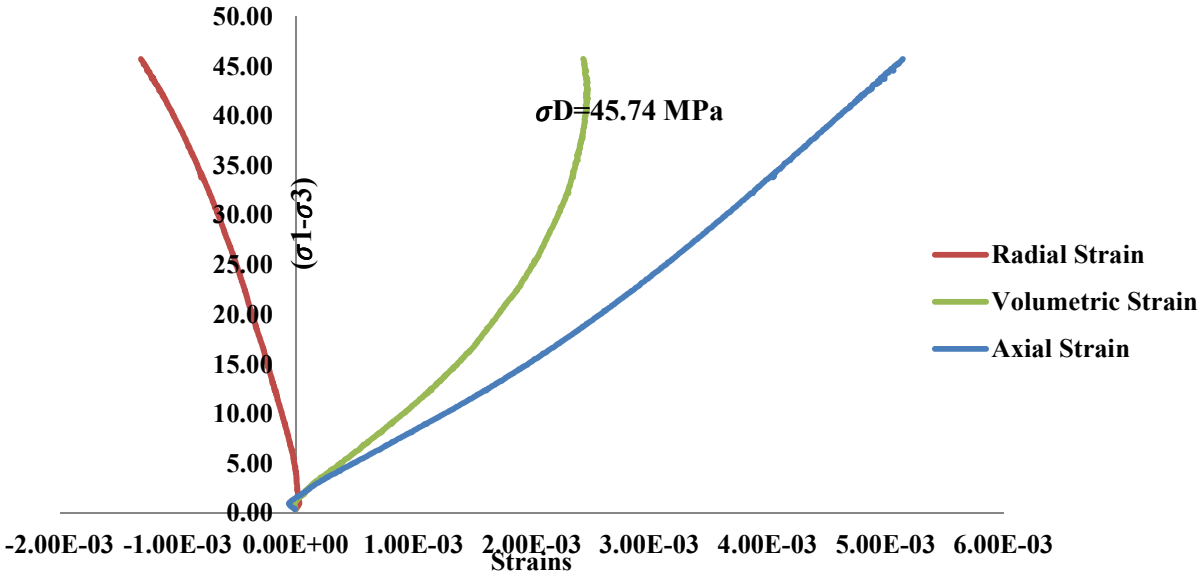

Figure 40: Stage 1 when Pc=3.44 MPa.

For the first loading stage a constant confining pressure of 3.44 MPa was used. It can be observed in Figure 40 that at the beginning of the test (the first 4 MPa) the specimen presented a nonlinear deformation that might be caused by the crack closure because the core was saturated at room conditions and not at a high pressure as the cases presented in the drained, undrained and unjacketed tests. For this stage the rock specimen was loaded until the volumetric strain in the stress-strain curve was totally vertical, meaning that after this stress condition the volumetric strain will change in direction as an indicative that the rock specimen will start dilating as a result of the microcracks presented in the structure of the rock.

The second, third and fourth stage of the multistage experiment were carried out at the confining pressure of 6.89 MPa, 10.31 MPa and 17.19 MPa respectively. The

stages were ran by following the same procedure as in the stage 1, while the only difference was that between the stages a pertinent amount of time was taken when the confining pressure was increased for the next stage. During this time the strains in the rock core were monitored, and the test was not started until there were not residual strains caused by unloading the specimen between stages. The maximum deviator stresses obtained for the second (Figure 41), third (Figure 42) and fourth (Figure 43) stages are 62.59 MPa, 97.14 MPa and 120.64 MPa respectively.

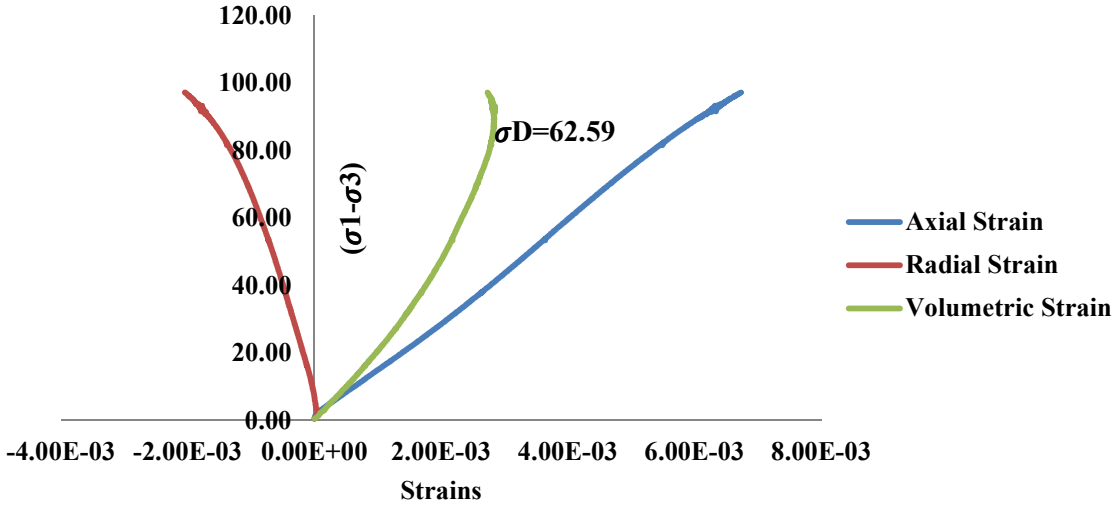

Figure 41: Second Stage of the multistage test.

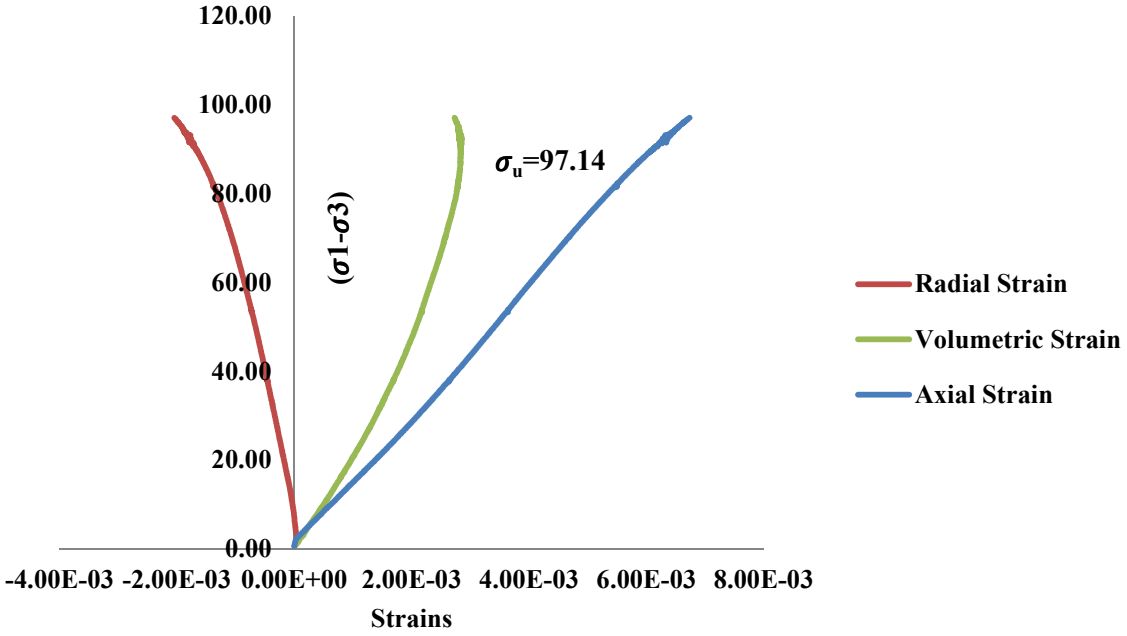

Figure 42: Stage 3 when Pc=10.31 MPa.

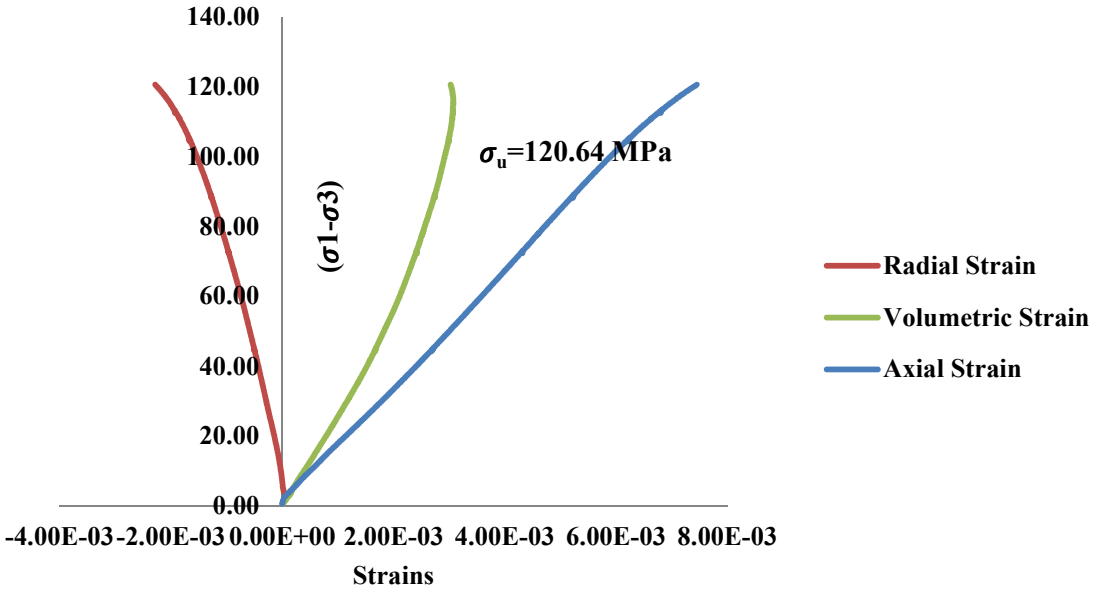

Figure 43: Stage 4 when Pc=17.19 MPa.

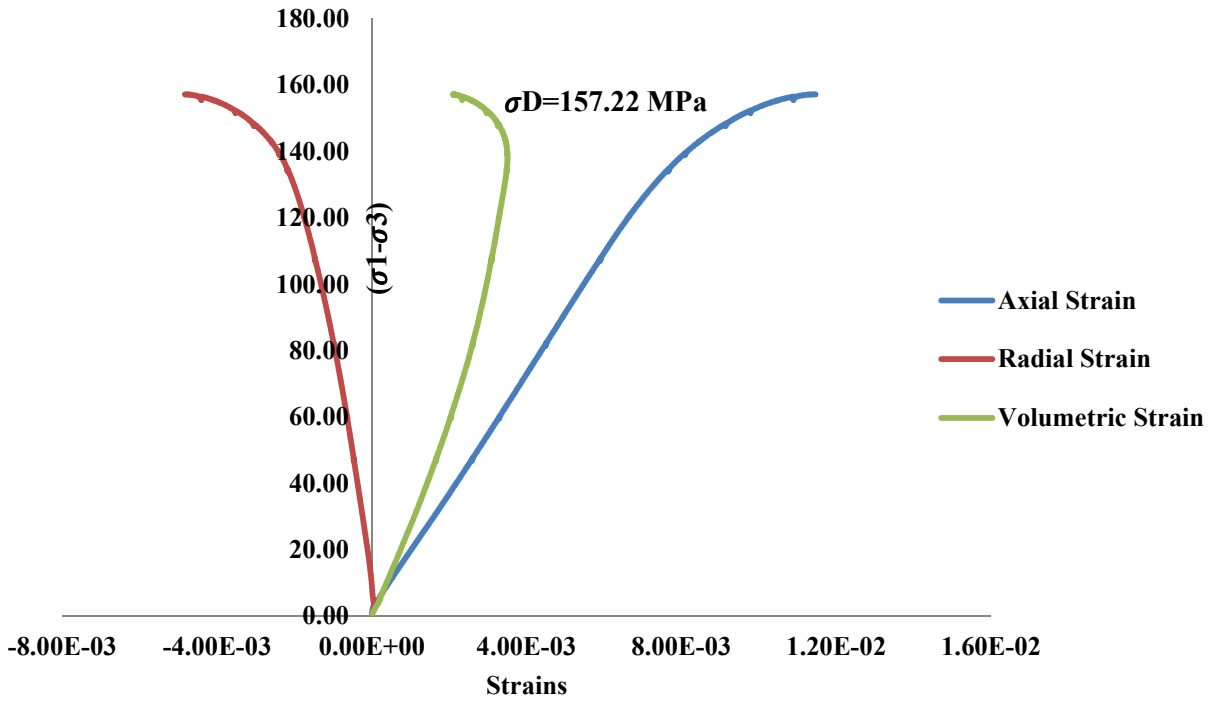

Figure 44: Final Stage for the multistage test in Berea Sandstone.

The fifth and final stage was performed at a confining pressure of 24.06 MPa after stabilizing the residual strains from the previous stages. In this stage it was allowed for the sample to fail, therefore we could observe the complete stress-strain curve with all the curve stages. It can be observed that after the slope change in the volumetric strain it continues increasing as negative strains, indicating that the sample will dilate due to internal cracks before failure. The ultimate load reached in this stage before failure is 157.22 MPa.

When the multistage test was completed all the information was collected and a Mohr envelope was constructed (Figure 45). This envelope was constructed by plotting in the abscissae the principal stresses σ_1 (σ_D and σ_c) and σ_3 (σ_c). Half of the difference

between the two principal stresses was used to obtain the maximum shear stress to draw the circle. After all the circles were plotted a tangent to all the circles was draw in order to determine the friction angle which was found to be 43°, noticeable higher than for water-wet tests. From this experiment we can conclude that using mineral oil as pore fluid result in strengthening of the material.

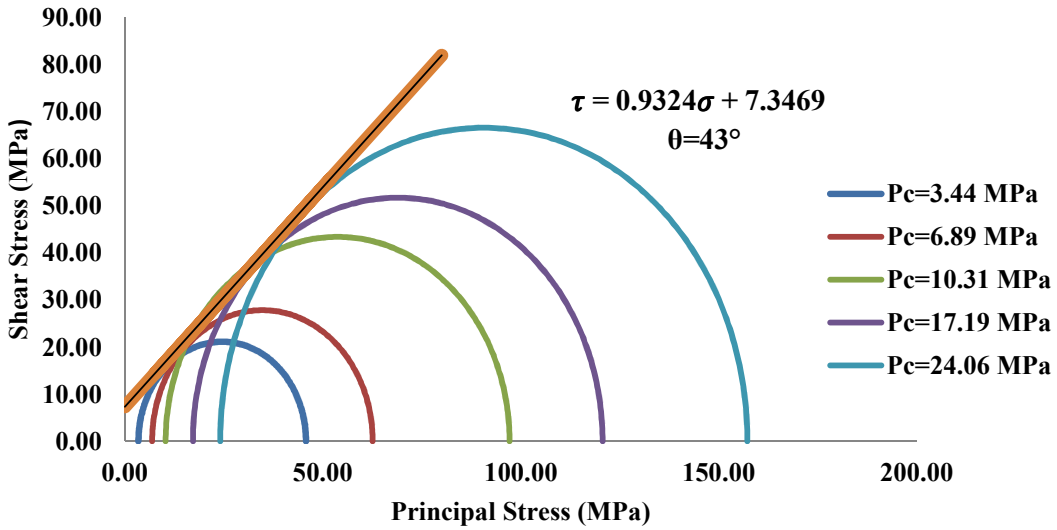

Figure 45: Mohr envelope for Berea Sandstone, using the multistage test.

6.4.2. Multistage Test in Westerly Granite

Another multistage test was performed in a purchased specimen, in Westerly Granite. For this rock the 5 loading stages were performed at the confining pressures of 3.47 MPa, 6.88 MPa, 13.75 MPa, 17.20 MPa and 24.10 MPa. The ultimate strength for

the first stage was 86.37 MPa (Figure 46), for the second stage was 134.88 MPa (Figure 47), for the third stage was 163.75 MPa (Figure 48), for the fourth stage was 197.2 MPa (Figure 49) and for the final and failure stage it was 241.10 MPa (Figure 50). Figure 51 shows the specimen used for this test, before and after failure.

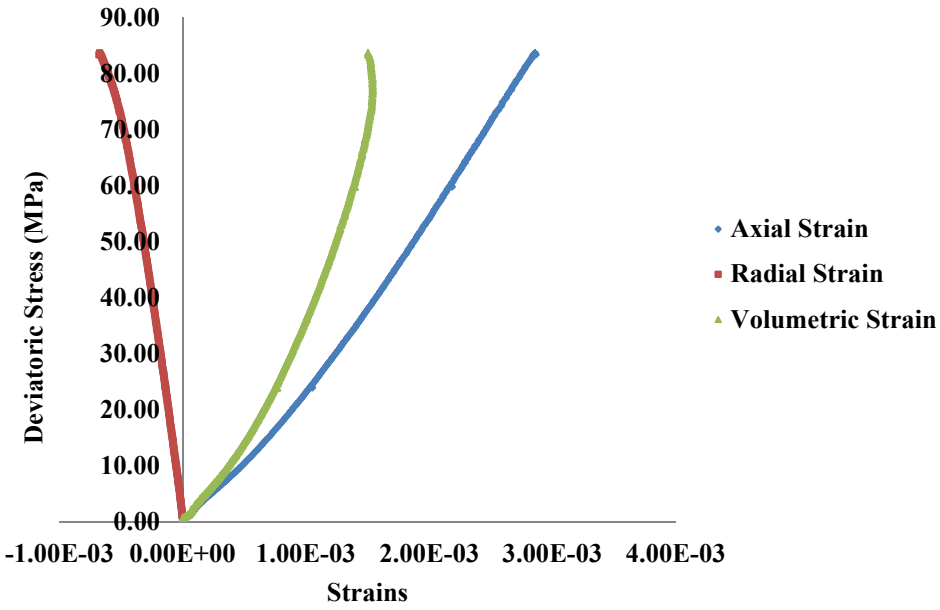

Figure 46: Stage 1 for the Westerly Granite, Pc=3.47 MPa.

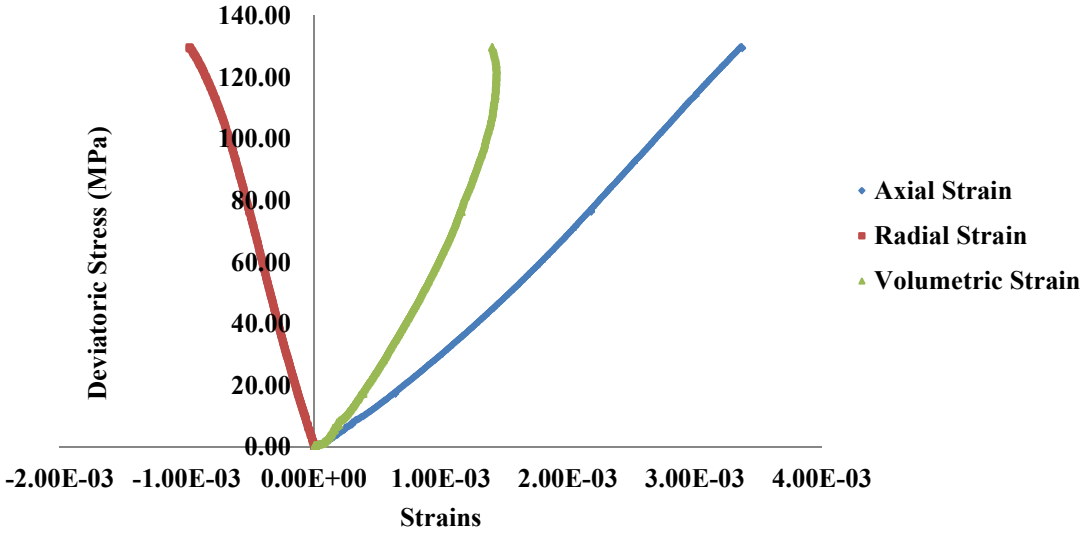

Figure 47: Stage 2 for Westerly Granite, Pc= 6.88 MPa.

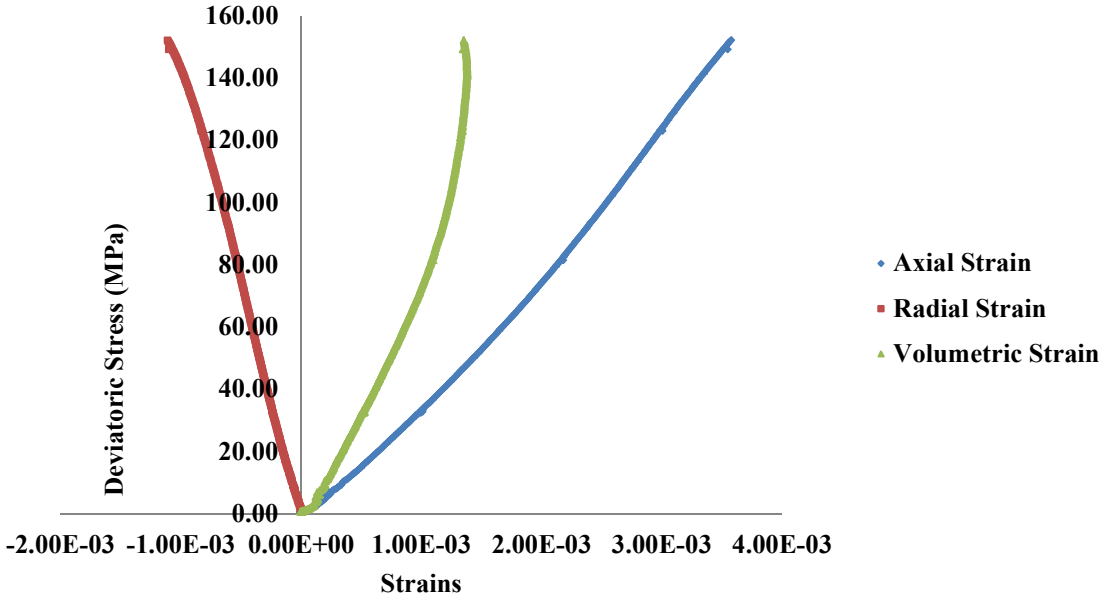

Figure 48: Stage 3 for Westerly granite, Pc=13.75 MPa.

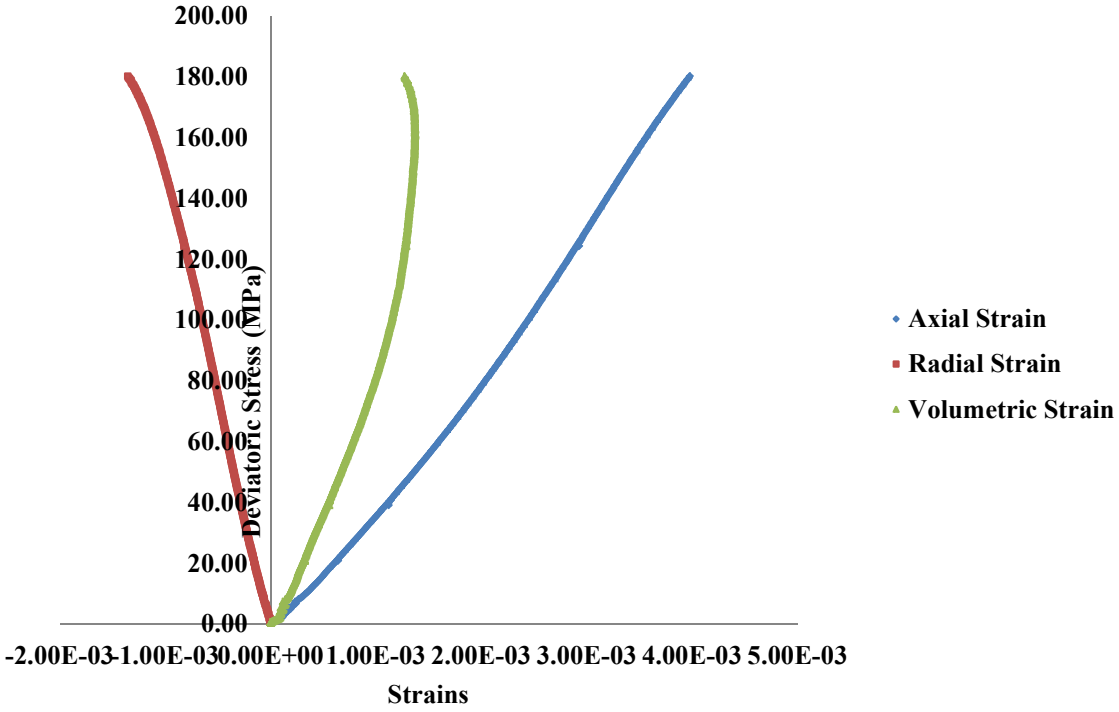

Figure 49: Stage 4 for Westerly granite, Pc=17.2 MPa.

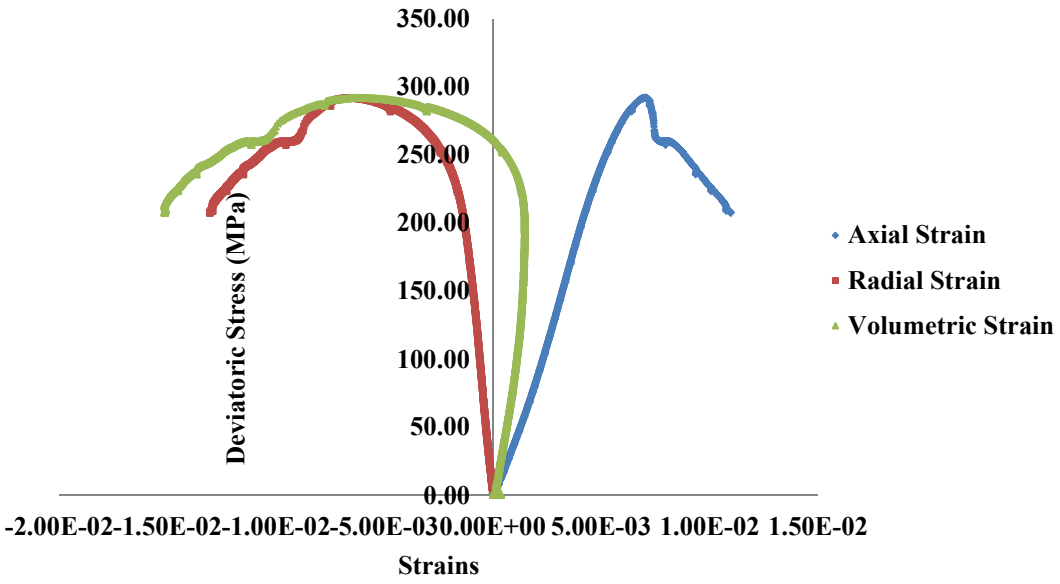

Figure 50: Final stage for Westerly granite, Pc=24.10 MPa.

Figure 51: Westerly Granite specimen before and after multistage test.

During the first four stages the deformation pattern was the same, while for the fifth it can be observed that the specimen experimented dilation that was as much as

double of the volumetric strain during the elastic range of the deformation. The friction angle obtained from the failure envelope constructed in Figure 52 was 55°, which is higher than the value presented in the literature for this type of rock. After completing both triaxial tests, it was observed that the angle of internal friction increased for mineral oil wetted rock for both cases, meaning that their resistance to shear decreases when mineral oil is used as a wetting agent and the rock weakened (Hadizadeh, 1991).

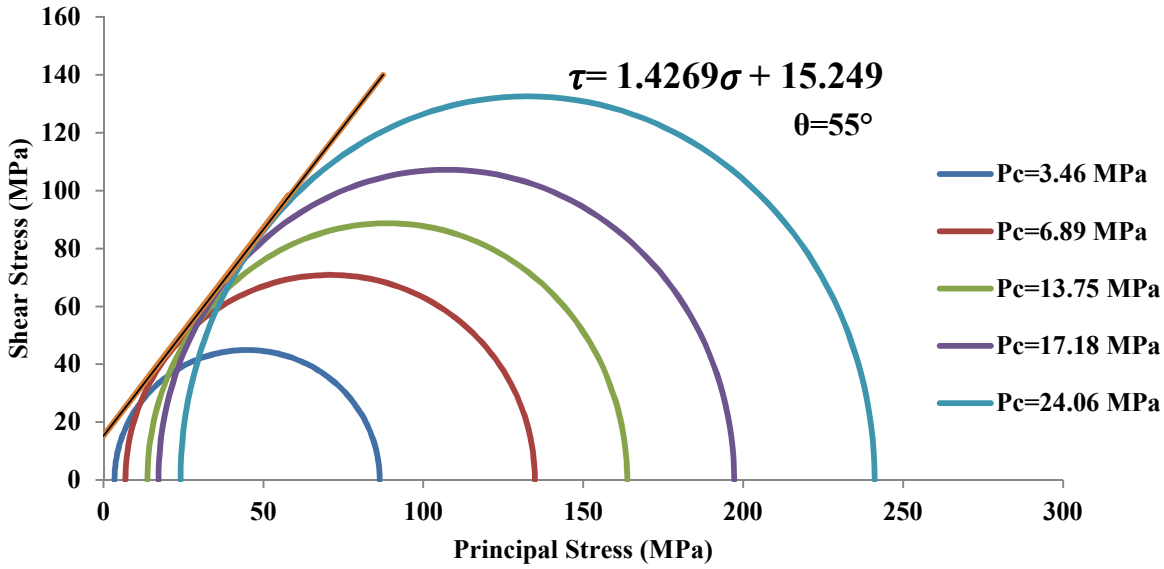

Figure 52: Failure envelope for multistage triaxial test in Westerly Granite.

7. CONCLUSIONS

An experimental characterization of the poroelastic geomechanical parameters for Berea Sandstone, Indiana Limestone, Westerly Granite and Welded Tuf was made to complete this project. It was observed that the poroelastic properties of the rocks depend on parameters such as mineral composition, transport properties, rock fabric and depositional environments, among others.

Biot's coefficient of effective stress α greatly depends on the stress level. At higher stress levels, the grain is less compressible and the pore fluid contributes substantially by carrying a great part of the external loads that affect the porous media. It was determined that multistage triaxial tests could provide a great deal of information of the mechanical parameters and that the knowledge of the mineralogy of the rock can help to determine other elastic properties.

It was observed that Skempton's pore pressure parameter B does not depends on the porosity of the rock, but of its conductivity and connectivity. It was also observed that in porous media the solid to fluid and fluid to solid coupling is not always present, leading to incompatibilities between the fluid and the solid.

REFERENCES

Akbarnejad - Nesheli, B., & Ghassemi, A. (2009). Undrained poroelastic response of berea sandstone and indiana limestone to confining and deviatoric stress change. *43Rd US Rock Mechanics Symposium,* Asheville, NC.

Anderson, O. L., & Nafe, J. E. (1965). The bulk modulus-volume relationship for oxide compounds and related geophysical problems. *Journal of Geophysical Research, 70*(16), 3951-3963. doi:10.1029/JZ070i016p03951

Bakhorji, A., & Schmitt, D. R. (2010). Laboratory measurements of static and dynamic bulk moduli in carbonate. *44th US Rock Mechanics Symposium,* Salt Lake City, Utah. *, 10-465*

Bargar, K. E., & Keith, T. E. (1999). Hydrothermal mineralogy of core from geothermal drill holes at newberry volcano, oregon. *USGS Numbered Series, Online version 1.0*(1578)

Biot, M. A. (1940). General theory of three-dimensional consolidation. *Journal of Applied Physics, 12*, 155-164.

Detournay, E., & Cheng, A. H. (1993). Fundamentals of poroelasticity. *Comprehensive Rock Engineering: Principles, Practice and Projects, 2*, 113. Oxford, UK.

Detournay, E., & H.D. Cheng, A. (Eds.). (1993). *Comprehensive rock engineering: Principles, practice and projects vol II*. Fairhurst: Pergamon Press.

Eithiraj, R. D., & Kalpana, G. (2012). Magnetism induced by nonmagnetic dopant in Li2O, Na2O, K2O and Rb2O: First-principles calculations. *Journal of Materials Science, 47*(5), 2316-2321. doi:10.1007/s10853-011-6046-y

Goodman, R. E. (1989). *Introduction to rock mechanics*. New York: Wiley.

Hadizadeh, J., & Law, R. D. (1991). Water-weakening of sandstone and quartzite deformed at various stress and strain rates. *International Journal of Rock Mechanics and Mining Science & Geomechanical Abstracts, 28*, 431-440.

Hart, D. (2000). *Laboratory measurements of poroelastic constants and flow parameters and some associated phenomena.* (Doctor of Philosophy, University of Wisconsin-Madison).

Hart, D., & Wang, H. (2010). Variation of unjacketed pore compressibility using Gassmann's equation and an overdetermined set of volumetric poroelastic measurements. *Geophysics, 75*(1), 9. doi:10.1190/1.3277664

Horváth-Szabó, G., & Høiland, H. (1996). Compressibility determination of silica particles by ultrasound velocity and density measurements on their suspensions. *Journal of Colloid and Interface Science, 177*(2), 568-578. doi:10.1006/jcis.1996.0071

I. Gil, B. A., G.G. Ramos, C.T. Montgomery, ConocoPhillips, Upstream Technology, & K Ormark, C. Soerensen, ConocoPhillips Norge. (2005). Failure mechanisms in deep-water chalks: Rock stability as function of effective stress and saturation. 40th US Rock Mechanics Symposium, Anchorage, Alaska .

Jamtveit, B., & Yardley, B. (1997). *Fluid flow and transport in rocks* (1st ed.). Oxford, Great Britain: Chapman and Hall.

Kobranova, V. N. (1986). *Petrophysics* (V. Kuznetsov Trans.). Moscow, Soviet Union: Springer-Verlag.

Kovári, K., & Tisa, A. (1975). Multiple failure state and strain controlled triaxial tests. *Rock Mechanics and Rock Engineering, 7*(1), 17-33.

Kumpel, H. J. (1990). Poroelasticity: Parameters reviewed. *Geophysical Journal International, 105*, 783-799.

Li, Y., Wang, J., Jung, W., & Ghassemi, A. (2012). Mechanical properties of intact rock and fractures in welded tuff from newberry volcano. *Thirty-Seventh Workshop on Geothermal Reservoir Engineering Stanford University,* Stanford, California.

Morrow, N. R., & Buckley, J. (2006). Wettability and oil recovery by imbibition and viscous displacement from fractured and heterogeneous carbonates. (No. DE-FC26-02NT15344). Laramie, WY: Chemical & Petroleum Engineering University of Wyoming.

Pagoulatos, A. (2004). Evaluation of multistage triaxial testing on berea sandstone. (MS, University of Oklahoma).

Q., L., Y., A., & R., L. (2006). Sound velocity measurements on K2O-Na2O-Al2O3-SiO2 liquids and the compressibility of crustal melts. *AGU Fall Meeting Abstracts,* , B1074. Retrieved from http://adsabs.harvard.edu/abs/2006AGUFMMR43B1074L

Richin, C. (Ed.). (1995). *Effect of stress variation onBiot's coefficient*. Norman, Oklahoma: University of Oklahoma.

Rouxel, T. (2007). Elastic properties and short-to medium-range order in glasses. *J.Am.Ceram.Soc, 90*(10), 3019-3039.

Selvadurai, A. P. S., & Shirazi, A. (2004). Mandel–Cryer effects in fluid inclusions in damage-susceptible poroelastic geologic media. *Computers and Geotechnics, 31*(4), 285-300. doi:10.1016/j.compgeo.2004.02.008

Skempton, A.,W. (1954). The pore-pressure coefficients A and B. *Geotechnique, 4*(4), 143-147.

Standard U.S.C. (2008). Standard practices for preparing rock core as cylindrical test specimens and verifying conformance to dimensional and shape tolerances. doi:10.1520/D4543-08

Terzaghi, K. V. (1943). In Chapman and Hall (Ed.), *Theorethical soil mechanics*. New York: John Wiley & Sons.

Thompson, M., Shen, X., & Allen, P. B. (2009). Density functional calculation of electronic structure and phonon spectra of Na2O. *Phys.Rev.B, 79*(11), 113108. doi:10.1103/PhysRevB.79.113108

Toseland, B. A., & Tischer, R. E. (1996). *Engineering development of slurry bubble column reactor (SBCR) technology.* (Quarterly Report No. 95051). Allenton, PA: Air Products and Chemicals, Inc.

Tran, D. T. (2010). Quantify uncertainty of rock failure parameters from laboratory triaxial testings using conventional and multistage approaches. *44th U.S. Rock Mechanics Symposium ,* Salt Lake City, Utah.

Vaidya, S. N., Bailey, S., Pasternack, T., & Kennedy, G. C. (1973). Compressibility of fifteen minerals to 45 kilobars. *Journal of Geophysical Research, 78*(29), 6893-6898. doi:10.1029/JB078i029p06893

Wang, H. F. (2000). Theory of linear poroelasticity with applications to geomechanics and hydrogeology. Princeton, New Jersey: Princeton University Press.

APPENDIX A

A.1 Poroelastic Paramaters

A.1.1 Skempton's Pore Pressure Parameter

A.1.1.1 Undrained Test

Prior to achieving a successful test, several experiments were performed using the original GCTS triaxial system, without making any modifications. The sample was prepared as described in the experimental procedure in Appendix A. After jacketing the specimen and installing the two axial and radial extensometers, the rock specimen was prepared for a cyclic loading to improve the linearity in the elastic regime by closing the microcracks with the applied stress. This was achieved by placing the specimen in the triaxial cell and loaded under hydrostatic stress at a constant load rate of 0.33 MPa/min, up to a value over 30 MPa. When the maximum value is reached, the confining pressure is also unloaded at the same constant rate.

Before starting the triaxial test, the jacketed specimen-stack is placed on the frame base and the confining cell is lowered by using the cell lift controller. After the cell is filled with confining fluid, the confining pressure is increased to 4 MPa, and then a deviatoric seating stress of 1 MPa is applied. Subsequently, the pore pressure is increased to 1 MPa. Two pressure gauges were installed in an independent inlet and an independent outlet to the cell pressure, with the purpose of recording pore pressure changes at both ends of the rock specimen. When the differential fluid pressure between the two gauges was less than 4%, the pore pressure was considered to be stabilized. The

pore pressure was provided with a system identical to the utilized for providing confining pressure to the triaxial system. In this system, the pressure transducer that measures the pore pressure is located in the pump that provides the pore pressure to the specimen.

In addition, two linear variable differential transformers (LVDTs) and one axial chain deformometer were installed to record the deformations. As observed in Figure 6, the two axial strain gauges were placed at 180^0 apart from each other, with respect to the cylindrical specimen, and the axial gauges were placed perpendicularly at the mid height of the rock specimen.

After the pore pressure was stabilized and the linearity in the rock specimen was improved, the rock specimen was loaded with a deviatoric stress of 1 MPa, at a constant rate of 0.33 MPa/min up to a pressure 30 MPa. During the test, the axial and radial displacements were recorded, as well as the instantaneous pore pressure at every new confining stress. It is important to note that the pore pressure is continuously monitored in the case it builded up more to a greater value than the confining pressure, and by this avoid the contamination of the confining fluid caused by the migration of the pore fluid out of the rock specimen.

After a series of tests were concluded, the same procedure was performed with Indiana Limestone, which is a a medium-fine grained sedimentary rock primarily formed by calcium carbonate and that has a unconfined compressive strength (UCS) of ≈ 34 MPa, according to steady state permeability tests measured by Kocurek Industries, Inc.

This type of rock has a considerable lower porosity of 14%, compare to Berea Sandstone and also a lower brine permeability of 9 mD to 14 mD.

A.1.2 Biot's coefficient of effective stress α

A.1.2.1K_o test

A four- stages test would be performed in order to calculate α directly from the experiments. During the first stage, a fully saturated rock specimen will be hydrostatically cycled three times from 2 MPa to 7 MPa at a constant rate of 0.7 MPa/min to simulate in situ conditions for the rock. After the cycling is over, the specimen will be loaded with a confining pressure of 7 MPa to 13 MPa and an axial deviatoric stress of 1 MPa to seat the sample and to prepare it for the axial loading that it will present in next stages. The pore pressure will be raised to 4 MPa and will be kept at this value along all the stages of this test. Biot's coefficient of effective stress α will be calculated using the same technique described above, but using a correction for the error in the fluid withdrawal.

The next stage of the test comprises the K_o test or uniaxial strain test. This test consists in loading the specimen under K_o conditions. The in situ K_o stress conditions means that the ratio of the effective horizontal stresses to the vertical stresses is such that no lateral deformation is presented in the rock mass and is constant for each type of rock. For this experiment, the axial actuator output will be set in axial strain control at a specific constant rate and the cell pressure output will be set at a constant value of lateral deformation (zero displacement) along the duration of this stage, which will finish By

doing this, the cell pressure will change at a constant ratio to the axial pressure, having the constraint of no lateral displacement. This stage will finish when the axial deformation is as much as twice the value of the confining pressure.

During the next and last stage of this test, the specimen will be set to hydrostatic conditions again, by increasing the confining pressure to the final value of the axial load from the previous step. The specimen then is loaded up to 40 MPa for the sake of equipment integrity (several components such as sealing glands and sealing O-rings can only hold up to 40 MPa). Then the pore pressure is released, and the specimen unloaded to complete the test. After the test is over, the coefficient of effective stress will be calculated by using the direct method explained earlier.

A.1.2.2 Expansion coefficient test

It is possible to determine poroelastic coefficient α by using the definition of alpha, as a product from original poroelastic parameters defined by Biot in 1941. As we can recall, alpha is defined,

$$\propto = \frac{K}{H}$$

Where *K* is the bulk modulus of the rock and *1/H* is the poroelastic expansion coefficient. To make this calculation effective, the test needs to be split into two stages. During the first stage, we will determine the bulk modulus by loading and unloading hydrostatically the rock specimen at a constant pore pressure. The bulk modulus will be calculated as stated below,

$$K = -V\frac{\delta Pc}{\delta V}$$

Where V is the bulk or total volume of the rock specimen, and Pc is the confining pressure at which the specimen is subjected. Bulk modulus K should be applicable to use to determine $\propto$, because it is a parameter independent from the pore pressure, but a property of the skeleton. For the next stage of the test the cell pressure will be held constant at different stress levels, and the pore pressure will be changed at a constant rate always keeping a safe positive effective stress to prevent migration of the pore fluid into the triaxial cell. At the time that the pore pressure is altered, the volumetric strain of the specimen is recorded. The poroelastic expansion coefficient *1/H* will be calculated as:

$$\left.\frac{\delta\varepsilon}{\delta p}\right|_{\delta Pc=0} = \frac{1}{H}$$

After K and 1/H are calculated, they are grouped for the correspondent stress level and then Biot's effective stress coefficient $\propto$ can be calculated.

A.2 Results

A.2.1 Undrained Test

After performing the test procedure described above, the results obtained are presented below, where it can be observed that the behavior of the pore pressure with respect to the change of applied confining stress. Figure 53 and Figure 54 show the pore pressure response as the confining pressure was increased for Berea Sandstone and Indiana Limestone respectively. Figure 53 also shows a plot of the *B* value vs confining pressure

and how it varies according to the ratio $\frac{V_{external}}{V_{pore}}$. This ratio is used as a metric to describe the results from different tests, and represents the ratio of volume of fluid external to the rock specimen to the volume of fluid within the rock core specimen. This ratio was utilized to see how the pore pressure response changed as the volume of external fluid was decreased in purpose. The same test was repeated for Indiana limestone, which has a permeability of about 6 times less than the Berea Sandstone. For both cases, the highest $\frac{V_{external}}{V_{pore}}$ is observed when no alterations had been made to pore pressure supply system and the lowest value is observed where the pore pressure supplier system was improved by changing the tubing diameter and length between the length communicating the pore pressure pump and the fluid within the rock specimen. The pore fluid pump was also changed from the pore pressure cabinet shown in Figure **5** to the Teledyne Isco 100 DM pump displayed in Figure **7**.

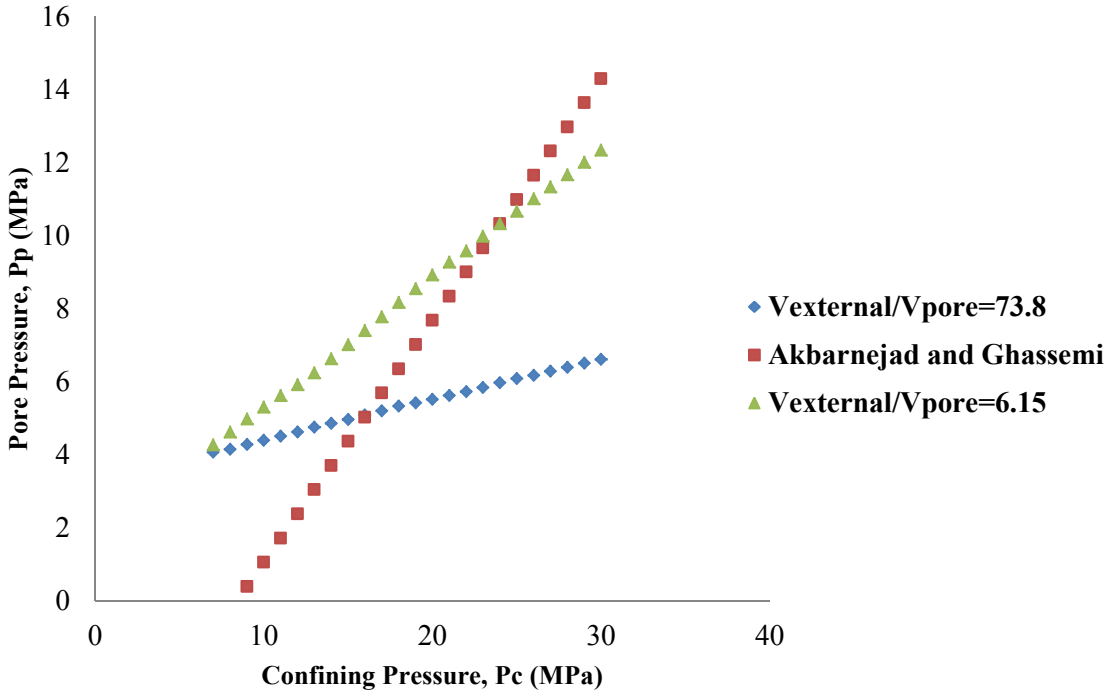

Figure 53: Undrained Test in Berea Sandstone.

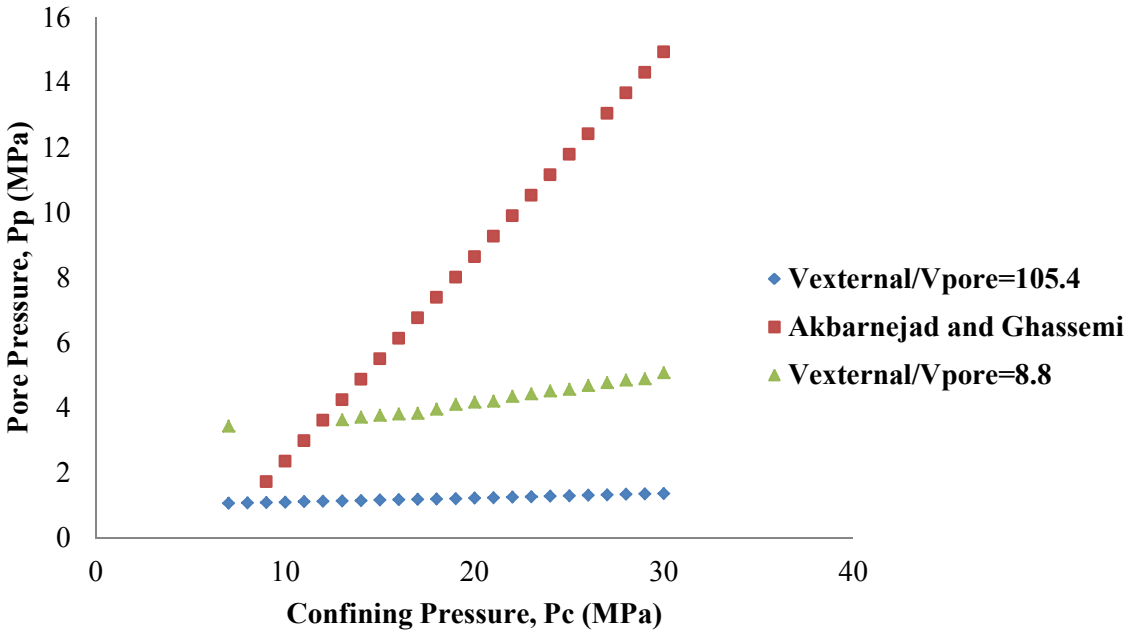

Figure 54: Undrained test for Indiana Limestone.

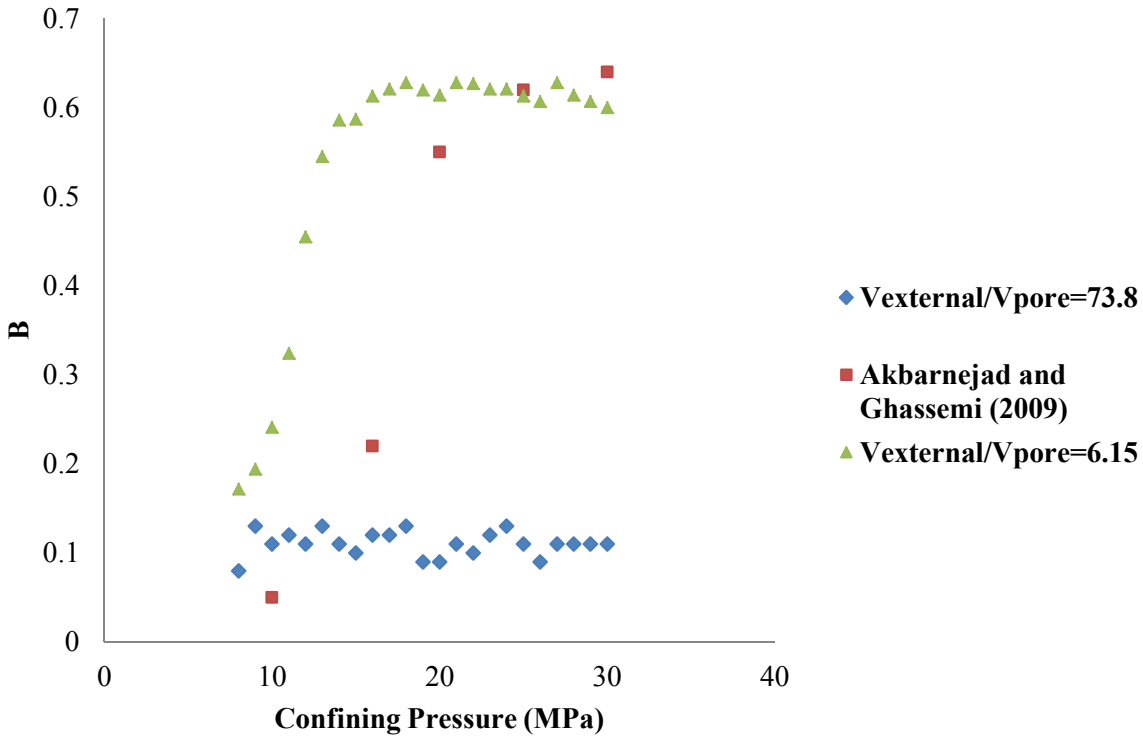

Figure 55: Skempton's pore pressure parameter for Berea Sandstone.

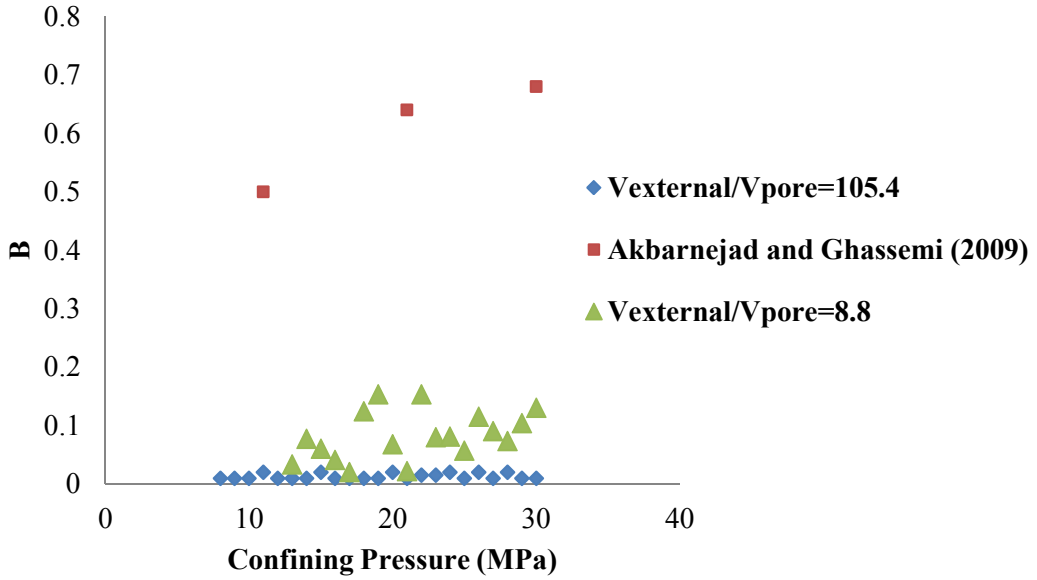

Figure 56: Skempton's parameter B in Indiana Limestone.

A.2.2 Drained Test

Hydrostatic Drained tests were completed using the same specimens. For both drained tests, the same saturation procedure described above was performed. For the drained test, the pore pressure was kept constant at 7MPa by injecting fluid at this constant pressure while loading, while the specimen was loaded hydrostatically at a constant rate of 0.33 MPa/min from an initial confining pressure of 10 MPa to a final pressure of 40 MPa. By increasing the confining pressure and leaving the pore pressure constant, the fluid was forced to migrate from the specimen. The volume of pore fluid expelled was recorded by quantifying the change in the reservoir volume in the syringe pump. Figure 57 and Figure 58 are displaying the volume of fluid expelled from the specimen against the

volume change in the specimen. Biot's coefficient alpha was calculated by computing the slope of this representation.

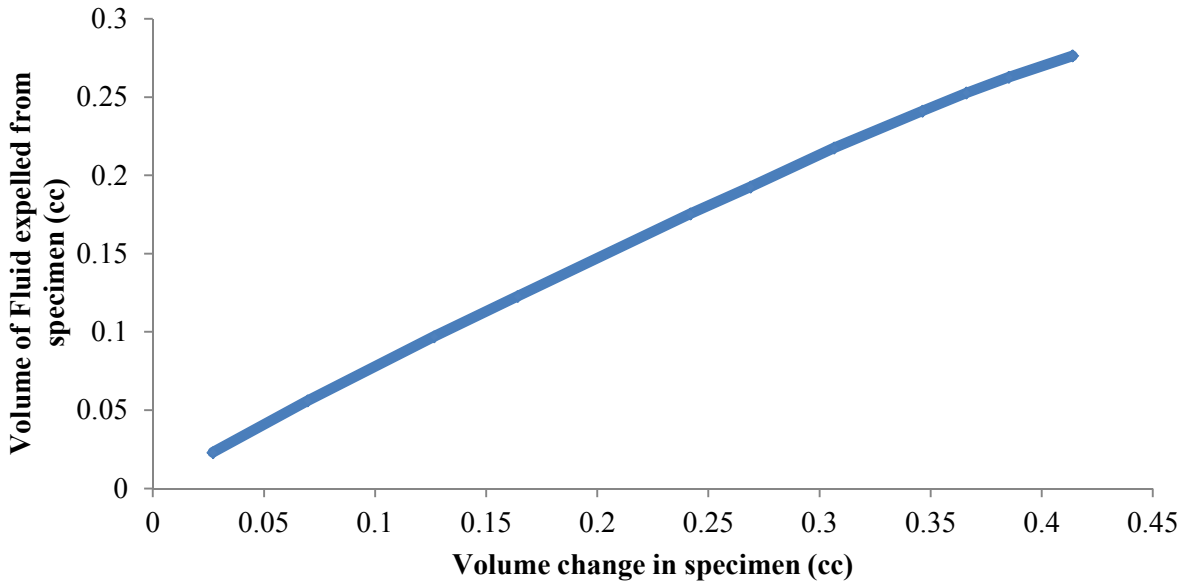

Figure 57: Volume expelled from the specimen for Berea Sandstone.

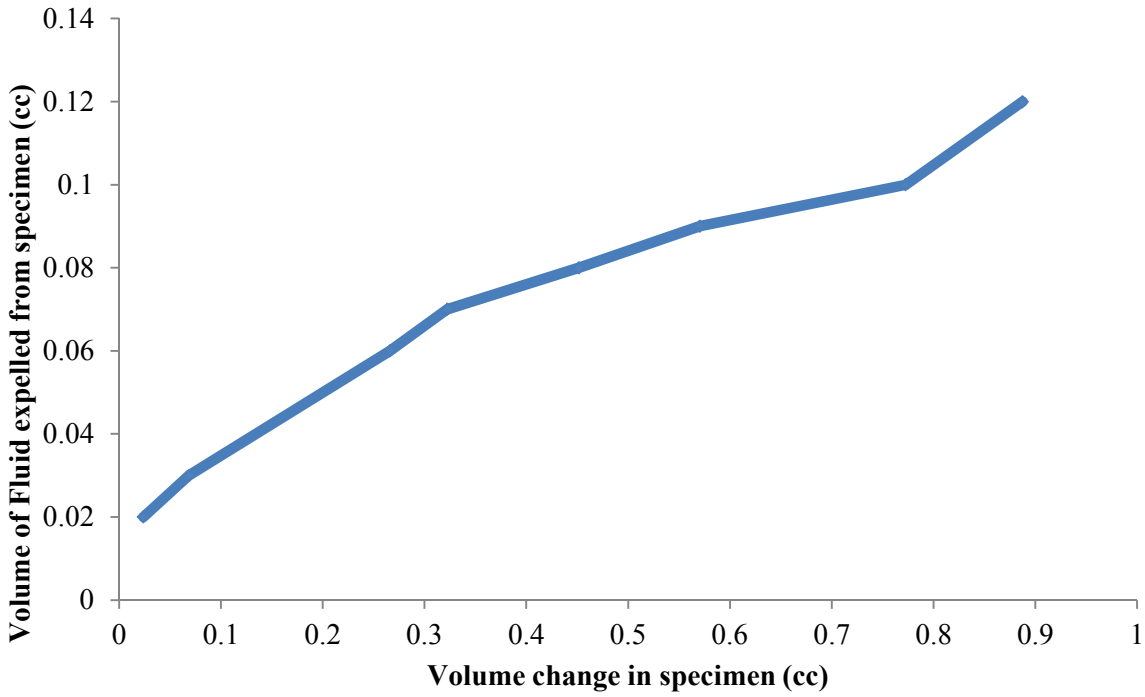

Figure 58: Volume expelled from the specimen for Indiana Limestone.

In Figure 59 and Figure 60 we can observe the numerical value of Biot's coefficient α for both of our specimens. As can be observed, the greater amount volume is mostly expelled at low confing pressures, which means that α decreases as the effective stress increases.

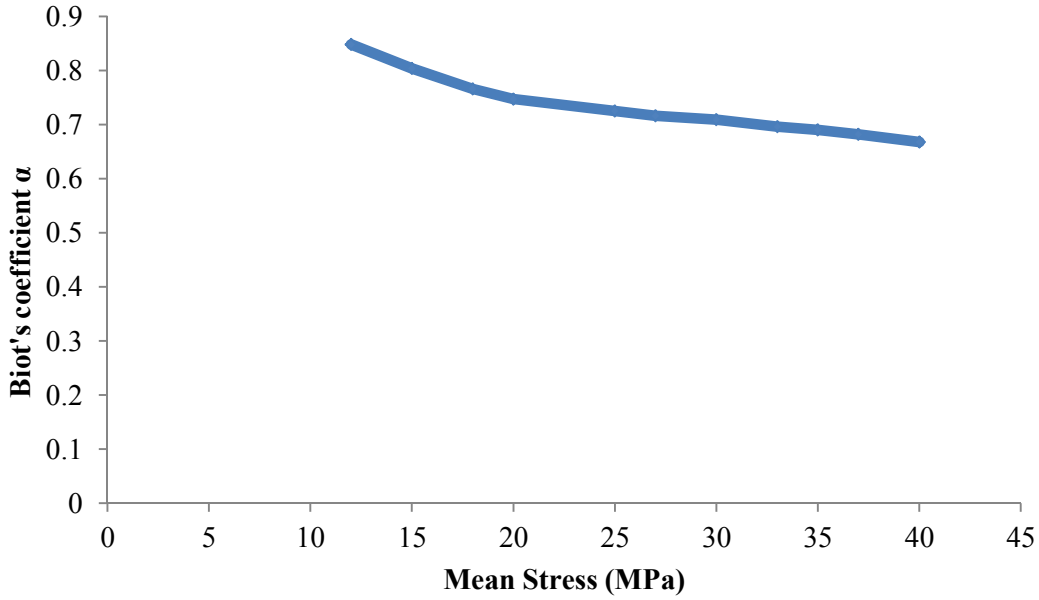

Figure 59: Biot's coefficient for Berea Sandstone.

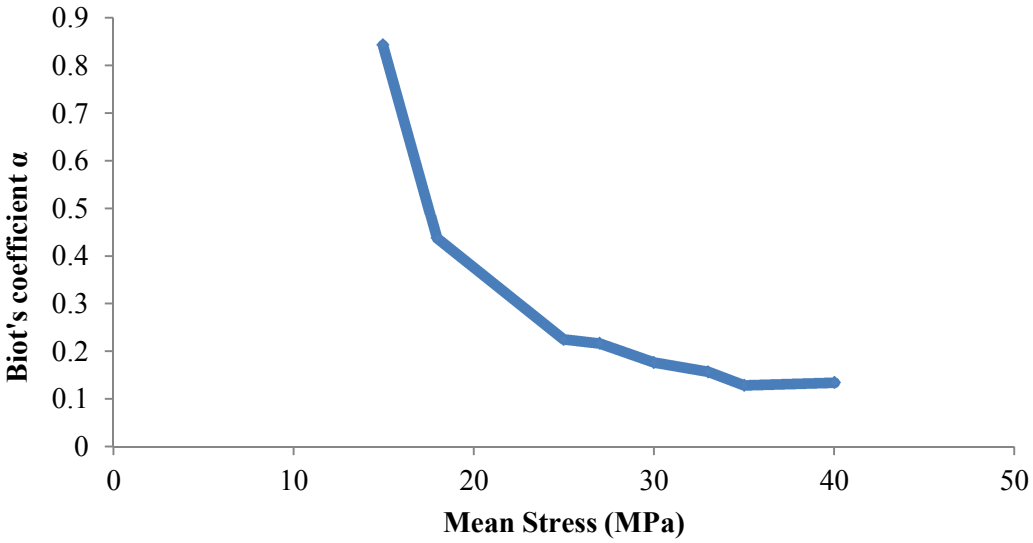

Figure 60: Biot's coefficient for Indiana Limestone.

A.3 Discussion and Comments for the Preliminary Results

The results obtained in tests for Berea Sandstone indicate that the external volume of pore pressure fluid that was in contact with the rock specimen influences the response of the pore pressure measurements, using both pore fluid systems. It is observed that as the $\frac{V_{external}}{V_{pore}}$ ratio is decreased by the aid of the Isco 100 DM pump, the response of the pore pressure transducer improved and is stable, and it can be represented by observing the increment of the pore pressure value "B". In the first test, when the ratio was 73.8, *B* value was not changing as expected as broadly observed in the experiments from the previous authors. By observing the pore pressure response plots, we can infer that there was no response at the transducer location to the change in the pore pressure which was located at the other end of the pore fluid hose, which is about 3 meters in length and 0.75 cm in diameter. However, when the ratio was reduced to 6.15, the response in the B values was observed to be similar to the values in existing literature. This reduction of the ratio was achieved reducing the communicating length to about 0.75 m and the tubing diameter to 0.158 cm. The rate at which the pore pressure changed as a result of a change in the confining pressure was compared to the results obtained by Akbarnejad and Ghassemi [2] in 2009. In our experiment the peak value obtained for *B* was about 0.64, while from Akbarnejad and Ghassemi was 0.68, within a range from 20 MPa to 30 MPa. The trend in both plots is similar, while the values at each confining pressure are different. This difference might be excused in the fact that the source of the two materials is not the same, between many other factors.

The same exercise was repeated for Indiana Limestone, but in this case the reduction of the volume did not worked as well, if compared to previously obtained results. When it was reduced to a ratio $\frac{V_{external}}{V_{pore}}$ of 8.8, and this might be because the permeability in the Indiana Limestone is several times lower than in the Berea Sandstone compared to previously obtained results. As our goal is to measure B and α for rock specimens with a porosity of about 2%, and permeabilities lower than the presented in Indiana Limestone, the system must be modified. It was evident that the external pore fluid affects the reading in the pore pressure transducer, and therefore, there was the need of reducing this volume as much as it is possible to achieve the correct measurements.

APPENDIX B

B.1 Experimental Procedure for the Poroelastic Tests

The different poroelastic tests will be carry out using the GCTS Triaxial System RTX-1500, with an Axial load capacity of 1,500kN and 140 MPa of confining stress capacity. The syringe pump Teledyne Isco 100 DM

B.1.1 Experimental Procedures

B.1.1.1 Core Preparation

3. Take a picture of the dry specimen.
4. Measure the dimensions of the sample according to the standard ASTM D4543-08.
5. Dry the sample at 100 degrees C for 14 hours.
6. Obtain the dry weight of the sample.
7. Saturate the samples in distilled water for 14 hours using the vacuum pump.
8. Obtain the wet weight of the specimen.

B.1.1.2 Test set-up

9. Mount the bottom platen in the cell.
10. Turn ON the SCON-2000 digital system controller. Open CATS GCTS software.
11. Turn on the hydraulic pump in low pressure (Low P Button), when the pore pressure or the cell pressure is below 50 MPa.

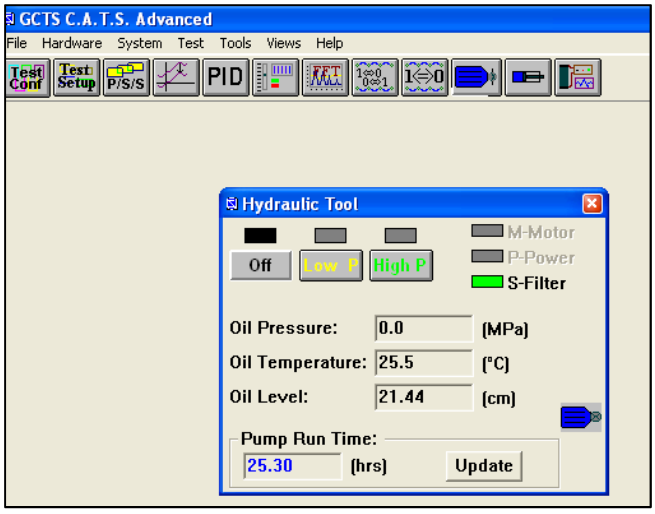

- Go to Outputs Function. Change to Pore pressure output and pore pressure displacement in the feedback. Reset pore pressure displacement and then turn the output function ON.

  Move the Set Point to a more negative point (-100). You will notice that the intensifier is filled up with water when the arrow indicator in the output function screen stops changing.

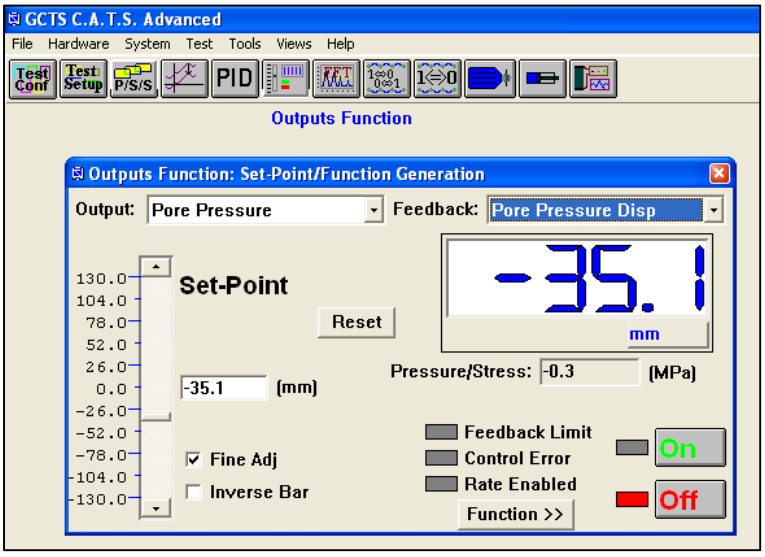

- Close the Dump Valve labeled “O”, open the Output Valve labeled N.
- Open pore pressure inlet in the platen and verify if the fluid is flowing by moving the intensifier up. Put the pore pressure fitting and move the intensifier. When water starts flowing, you will know that there is no air within, now you can put the pore pressure tube back in place and now you can install the sample.
- Remember to assemble the sample within the triaxial cell and not in the laboratory bench. The reason for this procedure is that the moisture can be controlled better in the cell, by maintaining closed the pore pressure outlets located in the platens.
- Install the core sample within the cell pressure. Use leaking protection in the platens as displayed below.

- Wrap the sample with Teflon tube. The Teflon needs to cover the sample and the top and bottom platens up to the pore pressure inlets, trying always to protect the orange band and the O-rings with the Teflon case.

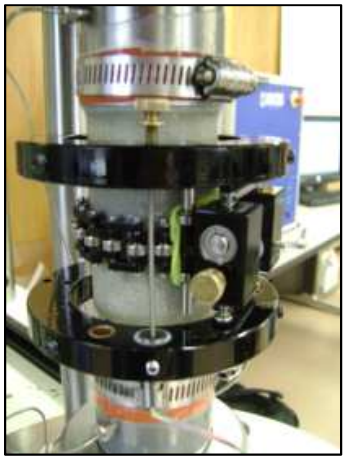

- Measure the gauge length. The gauge length is the distance between the top ring and the bottom ring. Take this distance from center to center of each ring.

- After having the core specimen installed in place, disconnect the pore pressure outlet in the top platen and follow the sample procedure did previously. Connect it back.
- Open the PV Outlet, located in the rear part of the bottom of the cell and move the pore pressure intensifier until water starts coming out.

B.1.2 Triaxial Poroelastic Test

B.1.2.1 Hydrostatic Test (Undrained, 1 MPa of deviatoric stress)

- Make sure that the air pressure valve that is next to sink in the main bench is open (parallel to the air line) and the pump breakers are in ON position.
- Load the screen Layout triaxial within the VIEWS window in the main program. Select the desired layout.

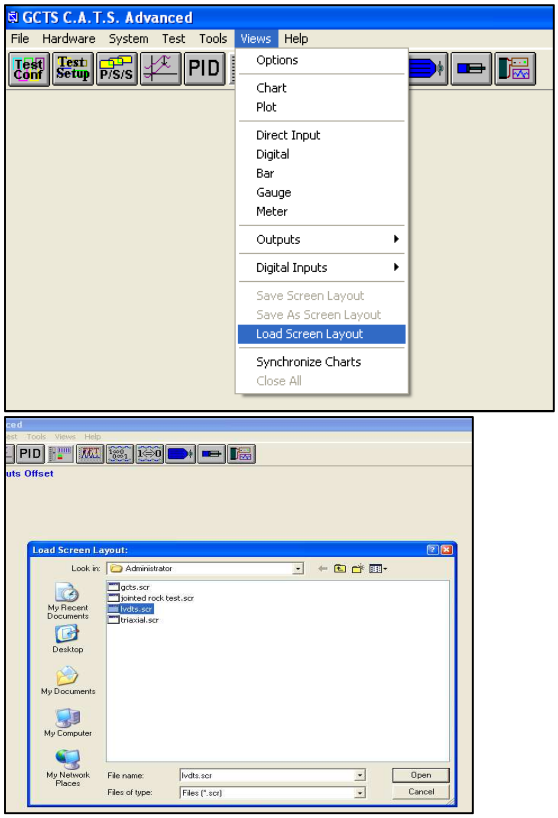

- Set the LVDT's 1, 2 and 3 to -2.0 mm, -2.0 mm and +2.0 mm respectively.
- Within the digital outputs control, turn the lift assembly on.

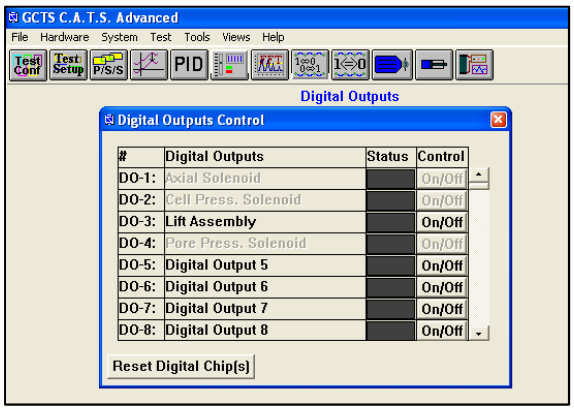

- Put the cell wall together with the cell. Disconnect the LVDT's cables from the front base of the cell.

- Turn the roller lift on and move the cell back under the load cell. Allow a few seconds for the roller lift in order to lift the cell up. Turn the roller lift off.
- Apply a 1 MPa deviator seating stress using the axial actuator within the outputs function with the axial displacement feedback. Remember to always turn the output function on before start operating. If the load cell is far apart to the piston, use the axial displacement feeback prior to using the deviatoric stress feedback.

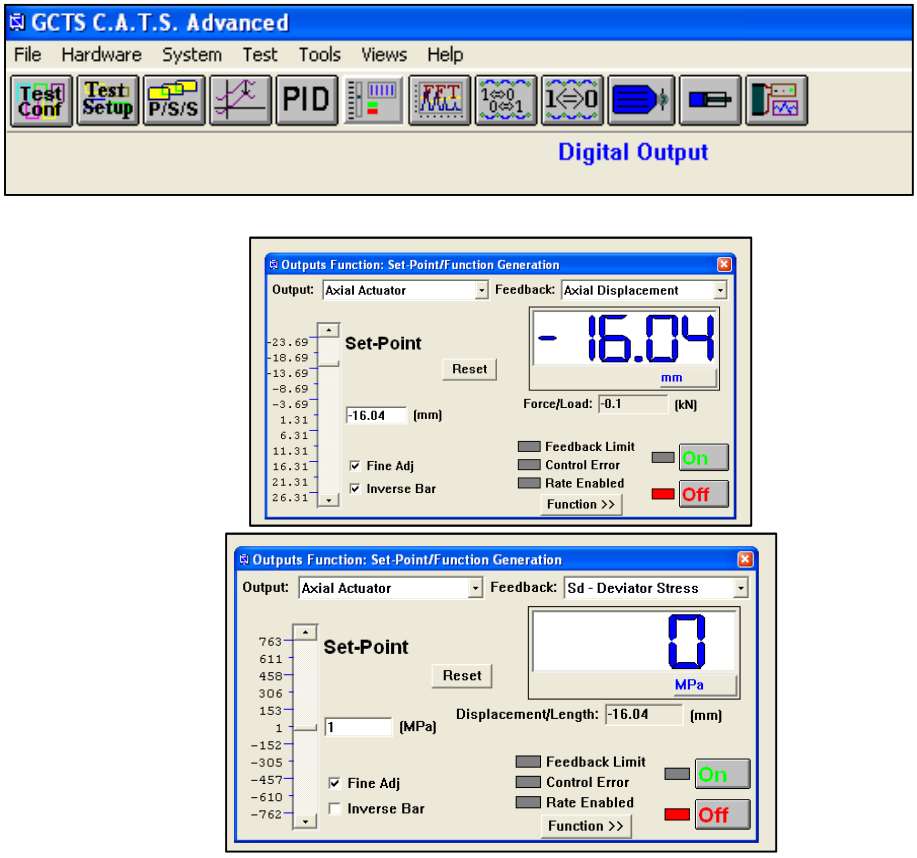

- Fill the cell with oil. Open everything in the cell pressure intensifier cabinet. Turn the air on. You will know that the cell is filled with oil when the cell

volume gauge is filled completely with oil. Close “B” and “D” valves, also turn the air on. The cell pressure will be around 0.4 MPa.

- Increase the cell pressure to make sure that the pore pressure will always be lower. Turn on the cell pressure output in the cell pressure feedback (6 MPa is a good value to start).
- Increase the pore pressure to 4 MPa in the pore pressure output within the pore pressure feedback. Always make sure that the pore pressure is lower.
- The specimen may have lost moisture during the set up. With the PV outlet close, inject water by controlling the pore volume rate, at a rate of 1 MPa/min and monitor the pore pressure. When pore pressure starts building up fastly, that is a hint that the sample is already fully saturated with water.
- Zero the LVDT’s.

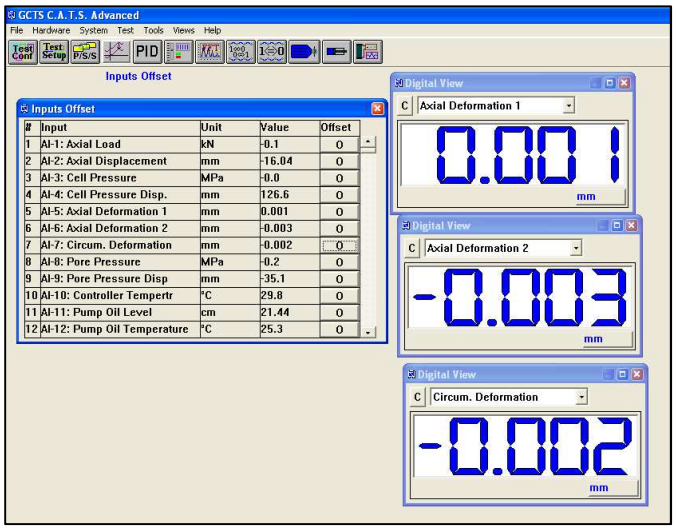

- Go to test configuration. Make sure the dimensions are corresponding with the actual specimen.

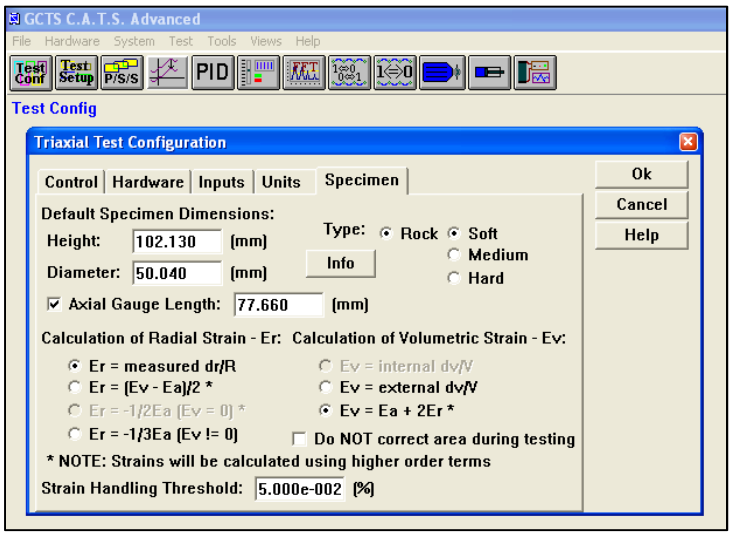

- Go to System-------→Configuration---------→Synchronize.

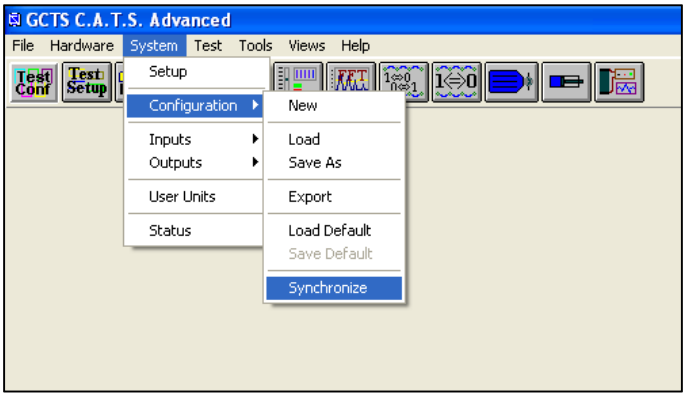

- Go to P/S/S----→Project---→ New sample

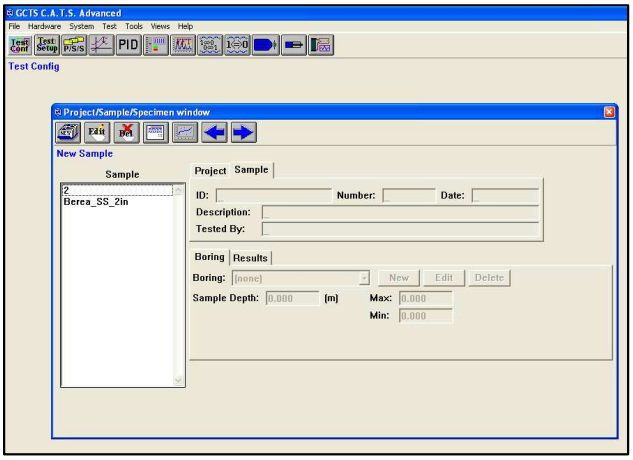

- Go to triaxial setup-------→Triaxial program definition---→Undrained test----→Cell pressure------Mode-----→ Constant or Rate. Set the final value.

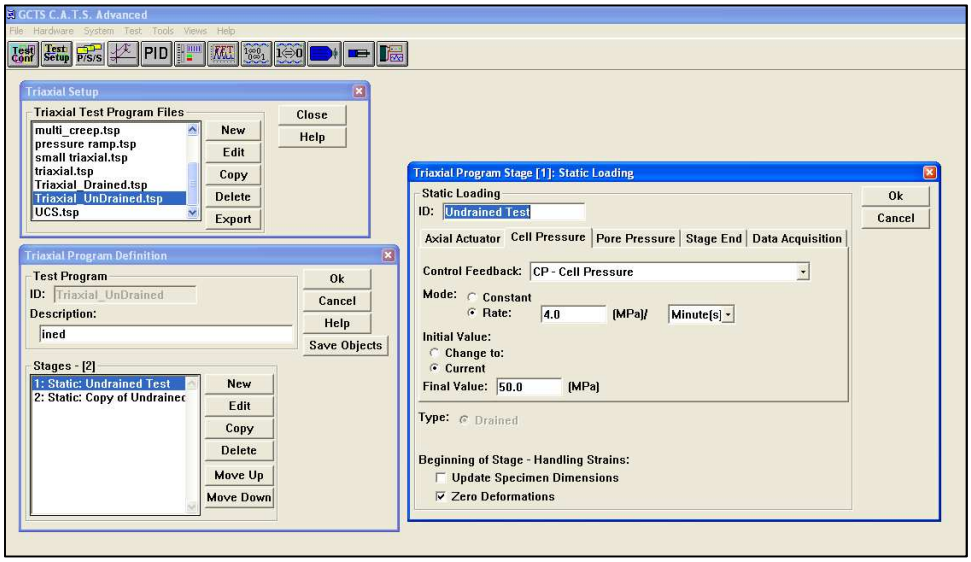

- Uncheck zero deformations in the actual deformation.
- Save objects in the triaxial program definition.
- Go to pore pressure. Control Feedback------→Pore Volume------→Mode Constant.

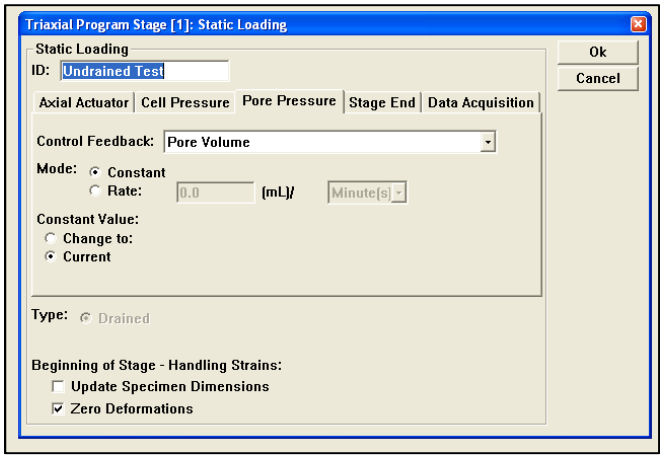

- Each valve in the pore pressure cabinet should remain open.
- For this undrained test, the fluid volume is not allowed to change. The pore Volume controller should be activated. Put everything into relative control. Switch control to displacement. Pore pressure intensifier to read what is happening inside.
- For the drained test, set pore pressure to 4Mpa and keep it constant. In this case the fluid volume change is going to be measured, while the cell pressure is ramping from 6 MPa to 40 MPa in both, load and unload.
- Go to file---------→ Configuration file---------→(Undrained test).
- Record the pore pressure values using while the cell pressure ramps.

B.1.2.2 Drained Poroelastic Test

Follow the exact procedures as they were set in the GCTS operation manual and in the Drained test (part A).

- Go to P/S/S--→Porotest-----→New specimen

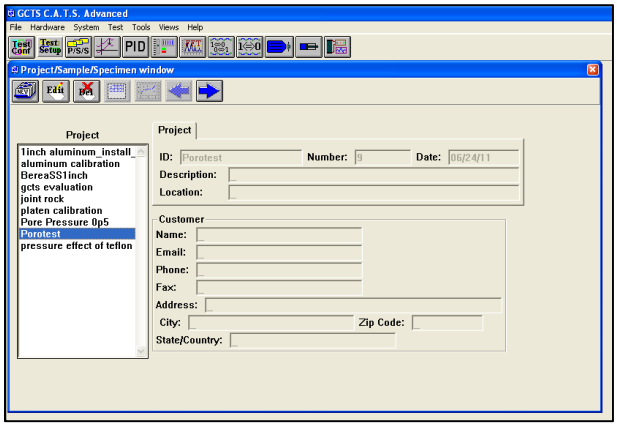

- Triaxial Setup→Control Feedback→Constant
- Go to triaxial program stage-→Static loading →
- Cell Pressure→Ramp Pore pressure →constant pore
- Make a copy of the Stage--→erase zero deformation.
- Cell pressure →control feedback → Cell Pressure Output →Cell pressure
- Zeroed the pore volumes
- Zeroed the LVDT's.
- Follow the procedure proposed for the drained test.